AIRS

Algorithm Theoretical Basis Document

Level 1B

Part 1: Infrared Spectrometer and Visible/Near-Infrared Channels

H. H. Aumann, Steve Gaiser and Mark Hofstadter
Jet Propulsion Laboratory
California Institute of Technology

Catherine Gautier and Shiren Yang
Institute for Computational Earth System Science
University of California, Santa Barbara, CA

Editor: H. H. Aumann

Technical questions regarding this document should be directed to the editor or to the authors of the major sections:

Table of Contents

1. Introduction

The Level 1b Algorithm Theoretical Basis Document (ATBD) describes the theoretical basis of the algorithms used to convert engineering units or data numbers from the Atmospheric Infrared Sounder (AIRS), the Advanced Microwave Sounding Unit (AMSU) and Humidity Sounder Brazil (HSB) to physical radiances. Engineering units or data numbers are referred to as a level 1a product, while the level 1b product has units of spectral radiance. The description of the algorithms which convert the level 1b measurements to geophysical units is covered in the Level 2 ATBD.

The Level 1b ATBD is divided into two parts:

- AIRS infrared spectrometer and visible/near-infrared channels

- AMSU/HSB Microwave channels.

The following document is the ATBD for the level 1b processing related to the AIRS infrared spectrometer and visible/near-infrared channels. This document assumes that the reader is reasonably familiar with the AIRS infrared spectrometer and visible/near-infrared photometer (Ref. 1.) and the AIRS Functional Requirements Document (FRD, Ref. 2). (Numbered references are listed at the end of Section 2.) Included in this document is a brief description of the relevant parts of the AIRS instrument necessary to explain references to devices, procedures and tables used by the level 1b algorithms. Version 1 of the ATBD assumes full compliance of the AIRS hardware with the AIRS FRD. Major revisions of the level 1b ATBD are anticipated in late 1997, based on the results of testing the partial AIRS Engineering Unit, and by late 1998, based on the results of the full characterization of the AIRS flight model.

1.1 Historical Perspective

The Atmospheric Infrared Sounder is a high spectral resolution IR spectrometer. AIRS, together with the Advanced Microwave Sounding Unit (AMSU) and the Microwave Humidity Sounder supplied by Brazil (HSB), is designed to meet the operational weather prediction requirements of the National Oceanic and Atmospheric Administration (NOAA) and the global change research objectives of the National Aeronautics and Space Administration (NASA). Limited characterization of the AIRS Engineering Model (EM) will start in April 1997. The AIRS flight model will be fully characterized in the summer of 1998, and integrated into the EOS-PM1 spacecraft. The three instruments will be launched in the year 2000 on the EOS-PM1 spacecraft.

The HIRS (High Resolution Infrared Sounder) and the Microwave Sounding Unit (MSU) on the National Oceanic and Atmospheric Administration polar orbiting satellite system have supported the National Weather Service (NWS) weather forecasting effort with global temperature and moisture soundings since the late 70's. After analyzing the impact of the first ten years of HIRS/MSU data on weather forecast accuracy, the World Meteorological Organization in 1987 (Ref. 3) determined that global temperature and moisture soundings with radiosonde accuracy are required to significantly improve weather forecasts. Radiosonde accuracy is equivalent to profiles with 1 K rms accuracy in 1 km thick layers and humidity profiles with 20% accuracy in the troposphere. This requirement is far beyond the capability of the HIRS sensor technology. Breakthroughs in IR detector array and cryogenic cooler technology by 1987 made this requirement realizable with technology available for launch at the end of this century. AIRS is the product of this new technology. AIRS, working together with AMSU and HSB, forms a complementary sounding system for NASA's Earth Observing System (EOS) to be launched in the year 2000. An integrated version of the three instruments, the Integrated Multispectral Atmospheric Sounder, IMAS, is expected to become the operational sounding system for the National Polar-Orbiting Operational Environmental Satellite System (NPOESS) to be launched early in the next century.

The measurement concept employed by AIRS/AMSU/HSB follows the concept originally proposed by Kaplan (Ref. 4) in 1959, verified experimentally ten years later using the Satellite Infrared Radiation Spectrometer (SIRS), and used operationally by the High Resolution Infrared Sounder (HIRS) and the Microwave Sounding Unit (MSU): temperature and moisture profiles are measured by observing the upwelling radiance in the carbon dioxide bands at 4.2 µm and 15 µm, and in the water band at 6.3 µm. Compared to the HIRS spectral resolving power of about 50, however, AIRS will have a spectral resolving power of 1200. The high spectral resolution gives sharp weighting functions and minimizes the contamination of temperature sounding channels by water lines, other atmospheric gases and surface emission. Correction for Earth surface emissivity and reflectivity can be obtained by observing selected surface channels distributed throughout the 3.8 µm - 13 µm region. Accurate retrievals under partly cloudy conditions are obtained by combining the infrared measurements with co-located microwave data from the AMSU (27-89 GHz) and the HSB (150-183 GHz).

The AIRS instrument represents a major step forward in PV:HgCdTe detector array technology and in long life, low vibration, Stirling/pulse-tube cryo-cooler technology. The AIRS hardware development phase has been underway since 1991, and considerable progress has been made since that time. The Preliminary Design Review (PDR) for the AIRS Instrument was held in January 1995. A test facility especially designed for AIRS will be used to accomplish a complete pre-launch spectral, spatial and radiometric calibration of AIRS. Testing of the Engineering Model, starting in late 1996, is expected to be completed in

the Summer 1997. The delivery of a Protoflight Model is expected in September 1998. AIRS is designed for an operating lifetime of 5 years, with hardware redundancy in all critical subsystems. The AIRS power and mass requirement, 256 Watts and 156 kg, respectively, are comparable to other instruments of this class and are easily accommodated on the EOS-PM1 satellite.

The Interagency Temperature Sounder (ITS) Team, with representatives from NASA, NOAA, the University of Wisconsin and DOD, was formed in 1987 to convert the NOAA requirement for radiosonde accuracy retrievals to measurement requirements of an operational sounder. After extensive efforts in data simulation and retrieval algorithm development, instrument functional requirements were established in the areas of spectral coverage, resolution, calibration (radiometric and photometric), stability, spatial response (including alignment, uniformity, and measurement simultaneity), and sensitivity. Sensitivity is expressed as Noise Equivalent Delta Temperature, NEΔT, referred to a 250 K target temperature. The Functional Requirements Document (FRD) (Ref. 2) has been under formal change control since 1992.

2. AIRS Infrared Spectrometer

The AIRS instrument, shown in Fig. 2.1, includes an infrared spectrometer and a visible light/near-infrared photometer. (The visible/near-IR photometer will be discussed in Section 3.) The AIRS infrared spectrometer employs a multi-aperture slit and is pupil-imaging, with spectral coverage from 3.74 to 4.61 μm, from 6.20 to 8.22 μm, and from 8.8 to 15.4 μm. The nominal spectral resolution is $\lambda/\Delta\lambda = 1200$. The spectrum is sampled twice per spectral resolution element for a total of 2378 spectral samples. A diffraction grating disperses the radiation onto 17 linear arrays of HgCdTe detectors in grating orders 3 through 11. In the following we focus on those AIRS spectrometer design aspects which relate directly to the inflight radiometric and spectral calibration.

Key to the spatial coverage and the calibration is the scan head assembly, containing the scan mirror and the calibrators. An exploded view of the scan head assembly is shown in Fig. 2.2. Every 2.667 seconds a scanline of IR data is produced, during which time the scan mirror rotates through a complete 360 degrees. The scan mirror motor has two speed regimes: During the first 2 seconds it rotates at 49.5 degrees/second, generating a scan line with 90 ground footprints, each with a 1.1 degree diameter IFOV. During the remaining 0.667 seconds the scan mirror finishes the remaining 261 degrees of a full revolution. Routine calibration related data are taken during this time. These consist of four independent views of cold space, one view into a 308 K radiometric calibrator, one view into a spectral reference source, and one view into a photometric calibrator for the VIS/NIR photometer (see Section 3).
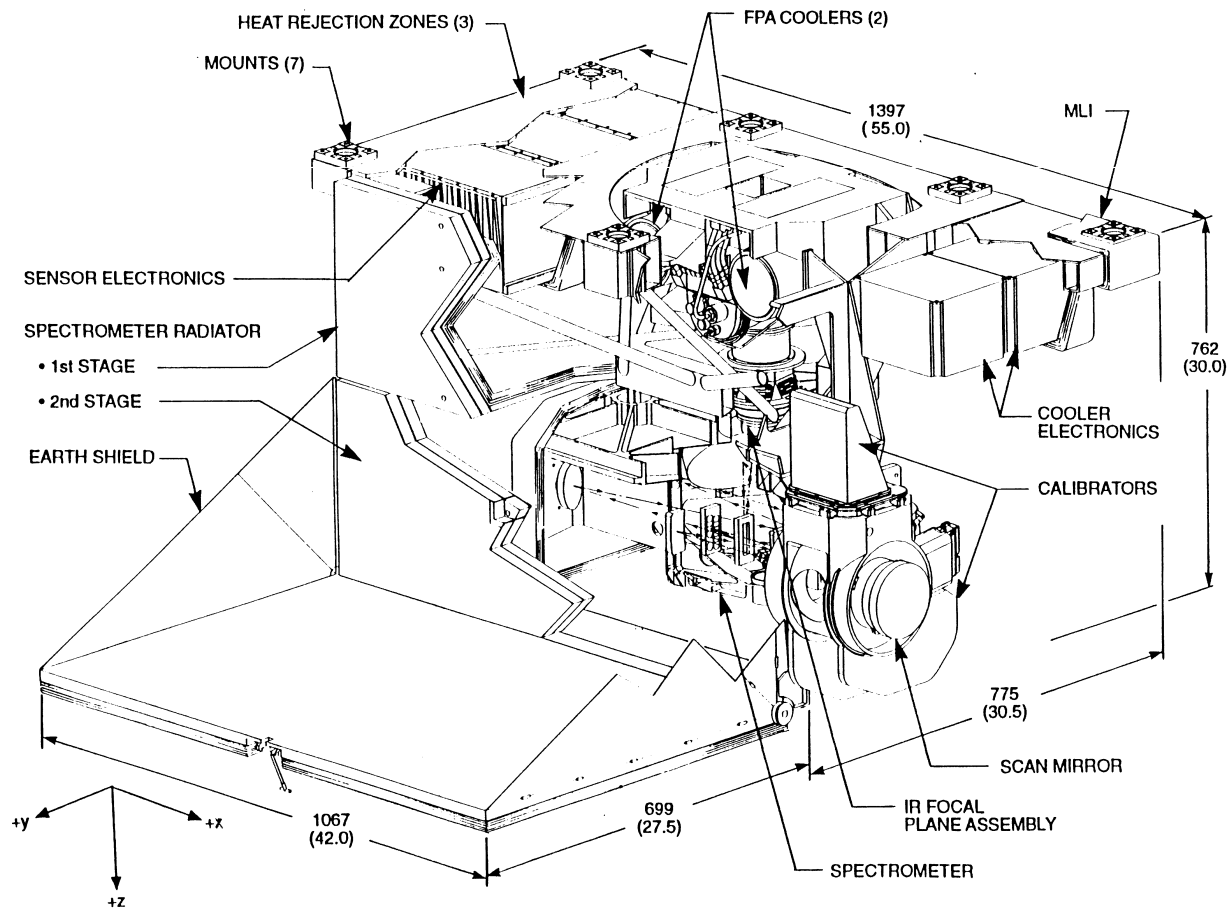
Figure 2.1

AIRS key hardware elements. The thermal blanket is partly removed to show interior details. The spectrometer is small compared to the volume required to support the space radiators, cooler and electronics.

The IR spectrometer is cooled to 155 K by a two stage radiative cooler. The IR focal plane is cooled to 58 K by a Stirling/pulse-tube cryo-cooler. The scan mirror is cooled to about 253 K (at beginning of life, 268 K at end of life) by radiative coupling to the Earth and space and to the 155 K IR spectrometer. Cooling of the IR optics and detectors is necessary to achieve the required instrument sensitivity. Signals from the detectors pass through onboard signal and data processing electronics, which perform signal amplification, radiation circumvention, offset subtraction, signal integration, and output formatting and buffering to the high rate science data bus. In addition, the AIRS instrument contains command and control electronics whose functions include communications with the satellite platform, instrument redundancy reconfiguration, the generation of timing and control signals necessary for instrument operation, and collection of instrument engineering and housekeeping data. The Stirling/pulse-tube cryo-coolers are driven by separate electronics which control the phase and amplitude of the compressor moving elements to minimize vibration and to accurately

control the temperature. Heat from the electronics is removed through coldplates connected to the spacecraft's heat rejection system.

Scan Head Housing

Motor-Encoder Assembly

Sun Shields
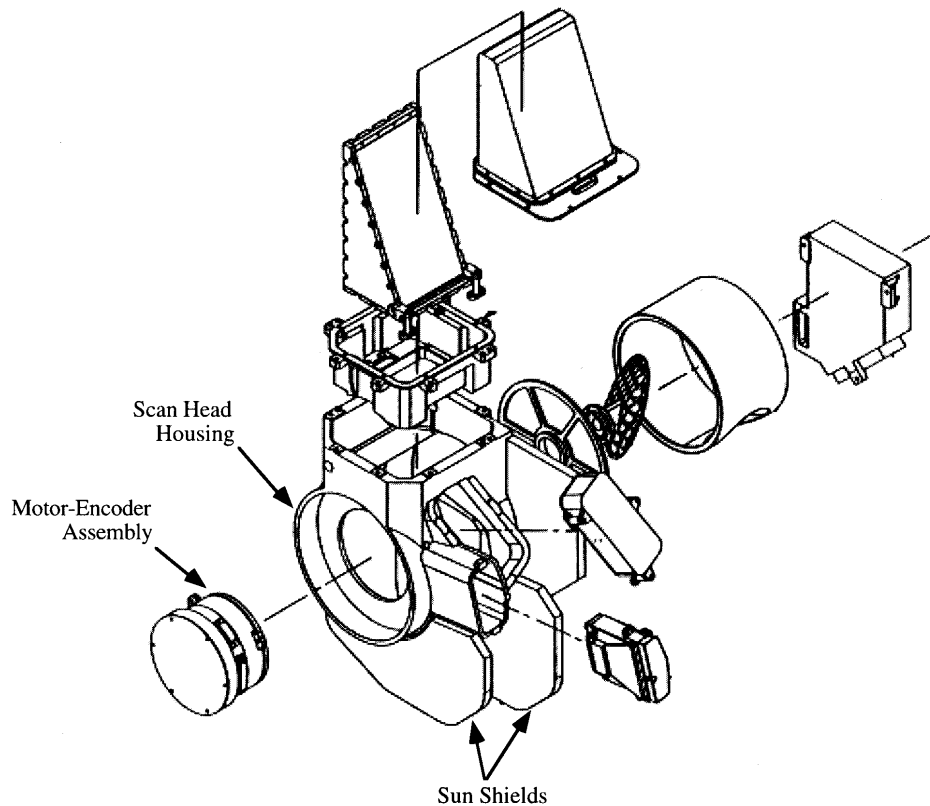
Figure 2.2

Exploded view of the AIRS scan head assembly. The scan mirror provides the cross-track spatial coverage, and generates a radiometric, photometric and space-view calibration every 2.67 seconds.

The multi-aperture and pupil-imaging spectrometer designs affect the calibration algorithm in different ways:

a) Located in the entrance pupil of the spectrometer are eleven apertures, which define the entrance slits (Fig. 2.3). These slits are spectrally dispersed by a grating. Each slit maps into one or two arrays on the AIRS focal plane. A single aperture in the image plane defines the spatial field of view at all wavelengths. This design virtually assures that all wavelengths measure the same spot on the ground at the same time. This measurement simultaneity is extremely important because clouds and water vapor are spatially highly variable. However, the design has the drawback that the entrance pupil is not circular, but looks like the projection of the eleven individual apertures (Fig. 2.4). As the scan mirror rotates to point the spectrometer field-of-view to the scene or to calibration sources, the projections of the entrance apertures trace out concentric bands on the surface of the scan mirror. The potential calibration error from this is discussed in Section 2.2.3.4.

b) Pupil imaging means that the entrance pupil (aperture) is imaged on the detector, instead of the scene. The detector response is not uniform over the detector area, but the entrance pupil is always uniformly illuminated. This design eliminates a potential scene illumination dependent spectral and radiometric calibration error.

ATMOSPHERIC IR SOUNDER ON THE EARTH OBSERVING SYSTEM
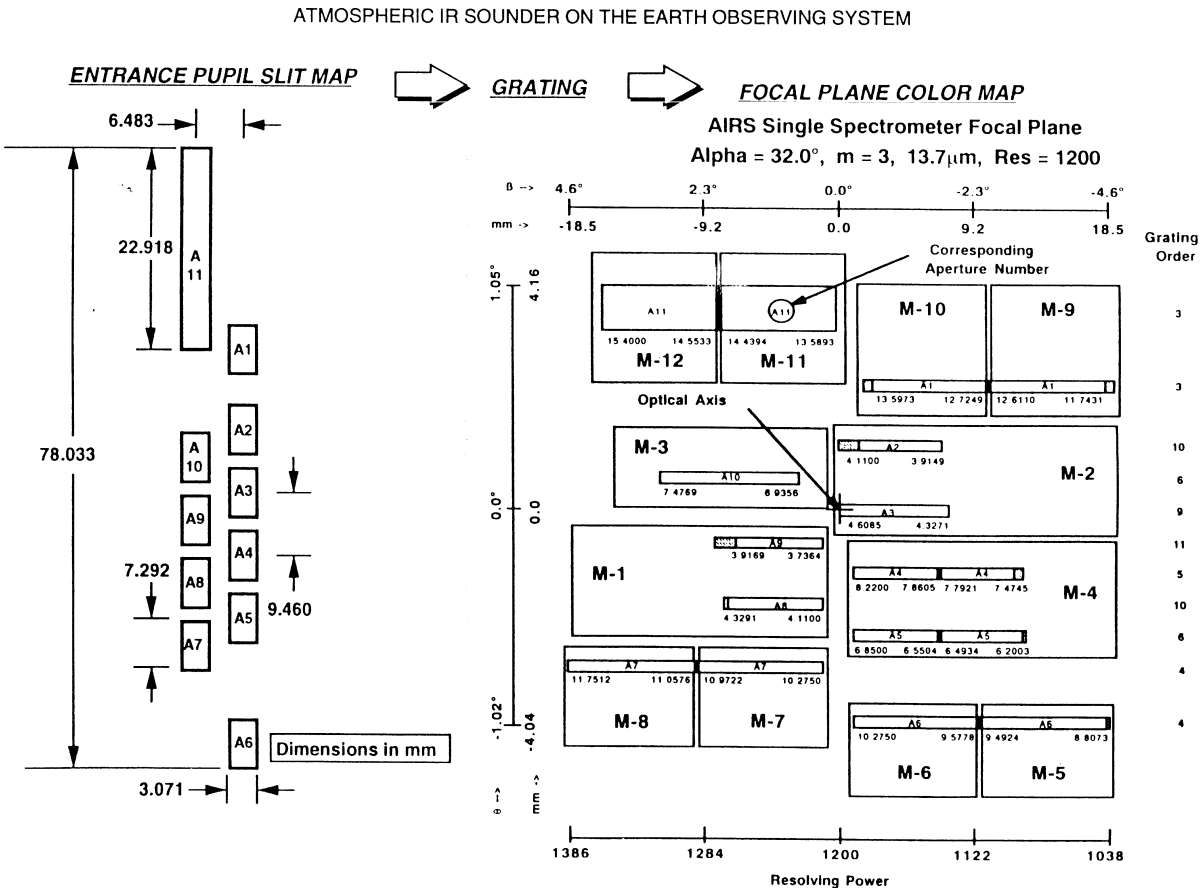
Figure 2.3

The eleven entrance apertures of the grating spectrometer are imaged onto linear arrays in the focal plane. All arrays and associated readout electronics are mounted on a single ceramic substrate. This greatly simplifies the spectral calibration.

2.1 Onboard Calibration Devices.

Routine calibration related data are taken while the scan mirror rotates from -49.5 degrees (relative to nadir) through 180 degrees (anti-nadir position) to +49.5 degrees. These data consist of four independent views of cold space, one view into a 308 K radiometric calibrator, one view into a spectral reference source, and one view into a photometric calibrator for the VIS/NIR photometer (see Section 3). The spectral reference source is a mirror coated with a thin film (about 100 microns thick) of Parylene. The spectrum of Parylene contains many well defined features which are useful for quick testing of

spectrometer functionality pre-launch. AIRS uses the Earth's upwelling spectral radiance for all spectral wavelength calibration.
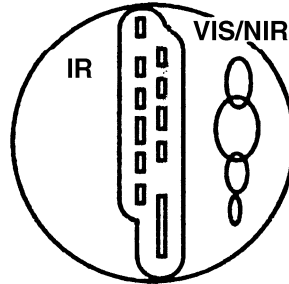
Figure 2.4

The projections of the spectrometer entrance apertures on the scan mirror.

2.2 Radiometric Calibration

The AIRS FRD calls for an absolute radiometric instrument calibration accuracy of 3% of the signal or four times the noise-equivalent radiance (NeN), whichever is larger, over the full range of expected effective target brightness temperatures (220 K to 350 K), and the full wavelength range covered by AIRS. This accuracy is to be maintained during five years in orbit.

In an ideal radiometer, incoming radiances and detector output readings are related through the calibration equation

$$N_{ot} = N_c \frac{V_t - V_s}{V_c - V_s} \ , \qquad\qquad \text{Eq. 2-1}$$

where N_{ot} and N_c are the radiances from the target scene and the calibration blackbody, respectively, and V_t, V_c, and V_s are detector outputs for the target scene, calibration blackbody, and space views, respectively. This equation is often stated as a combined detector/system gain

$$G = \frac{N_c}{V_c - V_s} \qquad\qquad \text{Eq. 2-2}$$

and

$$N_{ot} = G(V_t - V_s). \qquad\qquad \text{Eq. 2-3}$$

In order to meet the AIRS radiometric calibration requirements, the algorithm makes use of four major elements:

a) A linearization algorithm.

b) A zero-radiance-input smoothing algorithm.

c) The first order calibration equation (Eq. 2-1).

d) A polarization correction algorithm.

Details of the linearization procedure, which convert numbers to linearized engineering units are not discussed, but the residual error is part of the calibration error budget. An algorithm potentially needed to account for scan angle dependent scan emissivity is discussed, but is currently not part of the baseline calibration. Scan mirror emissivity variations, in the absence of a correction algorithm, are included in the estimation of calibration error. In the following we discuss instrumental details related to the theoretical basis for these algorithms.

For consistency with HIRS/2 instruments on the NOAA KLM series we have adopted units of mW/m^2 cm^{-1} sr for the AIRS level 1b spectral radiances. Each of the nineteen HIRS/2 channels can in fact be synthesized by summing about fifty AIRS channels weighted by the appropriate HIRS/2 spectral response function.

2.2.1 Cold Space View

The data number associated with a zero-radiance-input equivalent output data number is determined by means of the space view. The signal measured by AIRS viewing a ground target is the combination of the target radiance and the thermal emission from the AIRS instrument. Although the AIRS spectrometer is cooled to 155 K and the detector wavelength response is limited to 5% of the wavelength by interference filters cooled to the detector temperature of 58 K, emission from the instrument exceeds the signal from a typical target at all but the shortest wavelengths. Viewing cold space makes it possible to separate the instrument self-emission from target radiance. AIRS takes four space view measurements each scanline. The space views occur while the AIRS boresight vector is between 68.6 and 112.2 degree from nadir. These measurements are followed by a view of the blackbody. The cycle repeats every 2.67 seconds. In order to decrease the effect of observation noise in individual space views, space views are processed in a sliding window of about 5 minutes (TBD) length. Since the thermal time constants of the instrument components are of the order of hours, variations due to instrument emission are easily tracked.

In order to keep the electrical output of the detectors, for wavelengths longer than 6.9 microns, within the range of the 16 bit data word length, it is desirable to subtract from the output an offset value equal to the cold-space-view value plus V_o, where V_o is a small

fraction of the dynamic range. This is accomplished periodically (TBD, ground programmable period) by clamping the output of the electronics to V_o while viewing space view position number 2. The offset, V_o, is set prelaunch by a resistor, based on experience acquired during the calibration and characterization phase, as a zero offset of the ADC. This results in a data discontinuity (identified in the downlink data record) which is handled by the calibration software. This discontinuity is referred to as a "DC Restore". This restore is not required below 6.9 microns because the infrared background is much less than the signal from the scene. At wavelengths larger than 13.6 microns, the offset is removed by a tuning fork chopper.

2.2.2 On-Board Blackbody

The radiometric calibrator, shown at the top of Fig. 2.2, is a deep wedge cavity blackbody with a rectangular 5.7 cm by 9.5 cm clear aperture. The depth of the blackbody cavity is twice the diagonal of the clear aperture. The blackbody housing and cavity are made from beryllium to reduce its mass to 2 kg. The cavity walls are painted to maintain an emissivity higher than 0.91. An end-of-life blackbody emissivity of no less than 0.993 is obtained through multiple bounces of the light within the cavity. The deep cavity design and the multiple bounces make this design very insensitive to surface contamination during prolonged storage of the instrument on the ground or due to contamination in orbit. The blackbody is temperature controlled to 308 K using tape heaters. Temperature uniformity of the radiating surfaces is expected to be 0.07 K. Four dual redundant temperature sensors monitor the temperature at key positions in the cavity surface to an accuracy of 0.1 K. The blackbody is calibrated pre-flight relative to an external blackbody, a NIST traceable secondary standard developed by BOMEM, Inc., Quebec City, Canada. In order to minimize the single observation noise in individual calibration target views, blackbody views minus cold-space-views are processed in a sliding window of about 5 minutes (TBD) length.

2.2.3 Sources of Radiometric Calibration Errors

There are a number of instrumental effects which make the application of the ideal calibration equation discussed in Section 2.2. inappropriate. This presents two choices, each of which impacts the instrument design and/or the pre-launch testing:

a) Design the instrument (by specifying some components) such that the effects are small and can be absorbed in the AIRS absolute radiometric calibration budget.

b) Develop correction terms to the ideal calibration equation. The parameters in the correction terms (such as surface emissivities) must either be measured during pre-launch instrument characterization or must be calculable from in-orbit monitoring of additional components, such as temperature sensors.

Figure 2.5 shows the contribution of the three most important errors in the AIRS radiometric calibration: Blackbody output uncertainty, zero-point-offset error, and gain/offset coupled errors. These errors are residual errors, since suitable corrections are applied by the calibration algorithm. Different errors dominate in different wavelength regions. Based on the current knowledge of the subsystem performance, the first two error sources are adequately handled by first order corrections to the engineering units. The gain/offset coupled error requires a one step recursive correction by the calibration algorithm in spectral radiance domain. The root mean square of the uncorrected or uncorrectable residuals constitutes the absolute calibration error. The AIRS FRD requires that the root mean square of all error is less than four times the noise-equivalent radiance (NeN) over the full range of expected scene conditions.
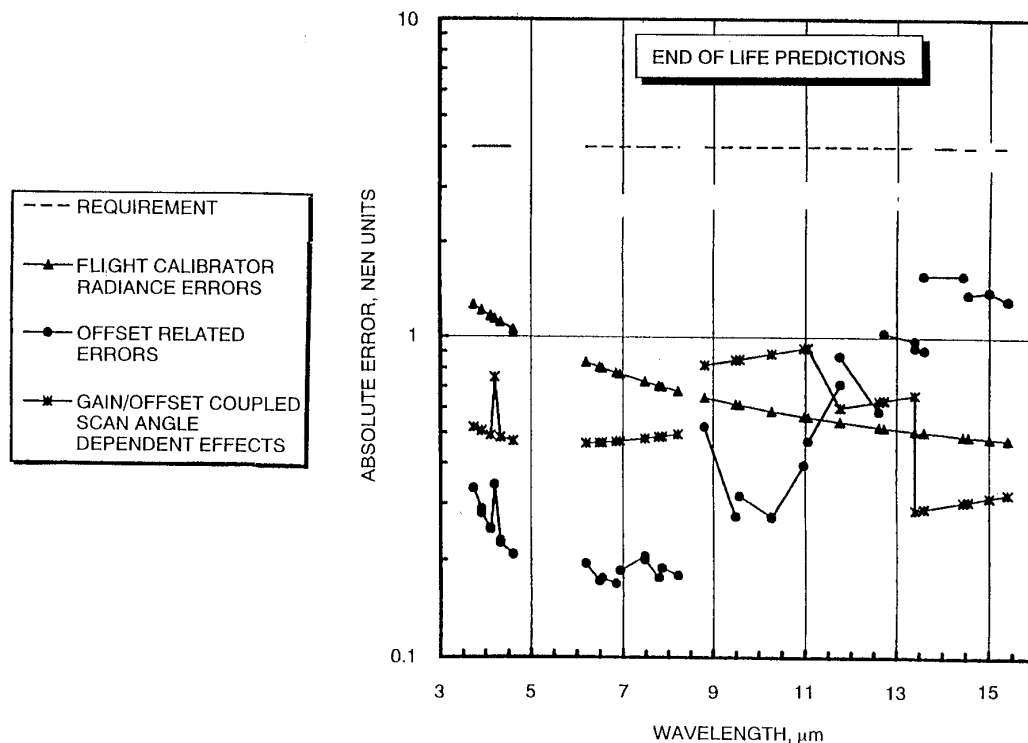
Figure 2.5

The predicted contribution of the most significant factors in the radiometric calibration uncertainty. Estimates refer to worst case, end-of- life conditions. Under all conditions the uncertainty is less than four NeN units.

2.2.3.1 On-board Blackbody

The on-board blackbody is a source of potential calibration error, but it turns out the estimated error is significant only at the shorter wavelengths. The accuracy of the knowledge

of the flight calibrator determines the accuracy of the knowledge of the average gain of the instrument. There are five terms affecting this accuracy:

a) Knowledge of the emitting surface temperature. Determining this requires knowledge of terms for the calibration of the temperature sensors, of gradients between the temperature sensors and the emitting surface, and of the accuracy in the electronics in reading out the sensor resistance. To get the temperature information, there are four sensors on the blackbody, and some effective temperature algorithm will be developed (based on flight model characterization) which pertains to each of the eleven AIRS apertures, since each aperture views a slightly different area within the blackbody cavity.

b) Knowledge in the effective cavity emissivity. This will be established by measurements of surface properties versus wavelength. Degradation of the characteristics in orbit are expected to impact the blackbody accuracy by less than 0.2% over the instrument lifetime.

c) Scattering of radiation from external sources that enters the blackbody cavity (from the scan mirror and scan mirror baffle). This effect is estimated to be small, changing the blackbody output by less than 0.1%.

d) Since the blackbody cavity has a finite aperture, the instrument, through its spatial out-of-field response, senses some of the radiation emitted and scattered from the exterior face of the aperture plate. The blackbody aperture is designed to enclose 99.5% of the AIRS beam. A black aperture plate, at a temperature of about 270 K, combined with the blackbody at 308 K, would produce a calibration shift of 0.4% at 4.0 microns, decreasing to 0.2% at 15.0 microns. The calibration uncertainty, after ground calibration, is less than these amounts. There is a temperature sensor on the aperture plate, but its reading is at present not included in the calibration algorithm.

e) A blackbody radiance uncertainty of less than 0.4% at short wavelengths, decreasing to 0.25% at long wavelengths, is assumed for the transfer of the NIST standard (using a NIST provided transfer radiometer) to the AIRS ground-calibration blackbody and from there to the flight blackbody.

2.2.3.2 Zero Point Offset.

The sources of zero point offset errors depend on the wavelength. The most significant offset error is due to stray light contamination of the cold space views. This has two variable components, one from the bright earth horizon (mainly sunlit clouds, which is a weather dependent factor) and one from the emissions and reflected sunlight from the side of the earth shield (sun angle dependent). Both depend on the angular position of the scan mirror and are significant at the shortest wavelengths up to about 5 microns.

2.2.3.3 Gain errors

Gain errors can be produced by non-uniform emission from the scan mirror due to contaminants on the scan mirror and/or scan mirror temperature gradients. This effect is caused by the shared aperture design. Figure 2.4 shows the projections of the spectrometer

entrance apertures on the scan mirror. As the scan mirror rotates, the apertures sweep out concentric bands on the scan mirror surface. Let N_s be the Planck function at the temperature of the scan mirror, and let ΔN_s be the change in that Planck function due to a temperature gradient across the scan mirror. Furthermore, let ε_s be the scan mirror emissivity in the space view position, ε_{ec} the emissivity in the blackbody view calibration position, and ε_{st} the emissivity in the target view positions. For the case of the AIRS instrument with a very low emissivity scan mirror and a small temperature gradient, we can neglect ε^2 end $\varepsilon * \Delta N_s$ terms. The calibration equation can then be expressed as

$$N_t = N_{ot}\left(1+\left(1+\frac{N_s}{N_c}\right)(\varepsilon_{st} - \varepsilon_s)\right),$$ Eq. 2-4

where N_t is the true target radiance.

If the rms deviation of the scan mirror emissivity from its mean value is $\Delta\varepsilon$, then the fractional radiance error is

$$\frac{dN}{N_t} = \Delta\varepsilon\left(1+\frac{N_s}{N_c}\right).$$ Eq. 2-5

The emissivity non-uniformity will increase with contamination level on the scan mirror and scan mirror temperature. Contamination will slowly build up during the five year mission to an estimated class 450 environment. Assuming a 266 K (end of life) scan mirror temperature with 2% mean emissivity and 0.2% rms emissivity non-uniformity, $dN/N_t = 0.28\%$ at 10 microns and 0.22% at 4 microns. At these levels no corrections need to be applied to the calibration algorithm and the error is absorbed in the calibration uncertainty budget. While the scan mirror temperature will increase over the life of the mission from 259 K to 266 K, the scan mirror temperature gradient is always expected to be less than 0.1 K over the mirror diameter, i.e., neglecting the $\varepsilon * \Delta N_s$ terms is valid. The scan mirror emissivity and temperature will be measured during the pre-launch characterization to validate the error estimate. The scan mirror emissivity variation will be measured during the AIRS flight model characterization.

2.2.3.4 Gain/Offset Coupled

Gain/offset coupled scan angle dependent errors occur when there is a scan angle dependent signal attenuation or a partially compensated scan angle dependent emission from the scan mirror. This error exceeds the on-board calibrator related error in the 8 - 12 μm region. The reason for this is the scan mirror coating. The AIRS scan mirror is made of beryllium, coated

with silver, overcoated by Denton Vacuum Inc. with a transparent protective coating. The process, FSS99, and the coating material are proprietary. This process produces a surface with very high reflectivity, excellent cleanability properties, and a proven durability record for prolonged space application. However, the overcoating also produces a small amount of polarization in the 8 - 12 μm region. Figure 2.6 shows a tracing of the spectral reflectivity for s- and p-wave polarization between 7.5 and 15.5 μm relative to the reflectivity of pure gold. The effect is strongest at 8.8 μm, where the s-wave reflectivity is 98%, but the p-wave reflectivity is only 86%. The polarization vector rotates with the rotation of the scan mirror. Thermal emission from the atmosphere is not polarized. Since the AIRS instrument transmission is polarization dependent, the combination of the rotating scan mirror and the instrument creates a polarizer/analyzer effect. In the following we analyze the magnitude of this effect and show that it can be reduced to a negligible amount using first order correction terms obtained from pre-launch characterization.
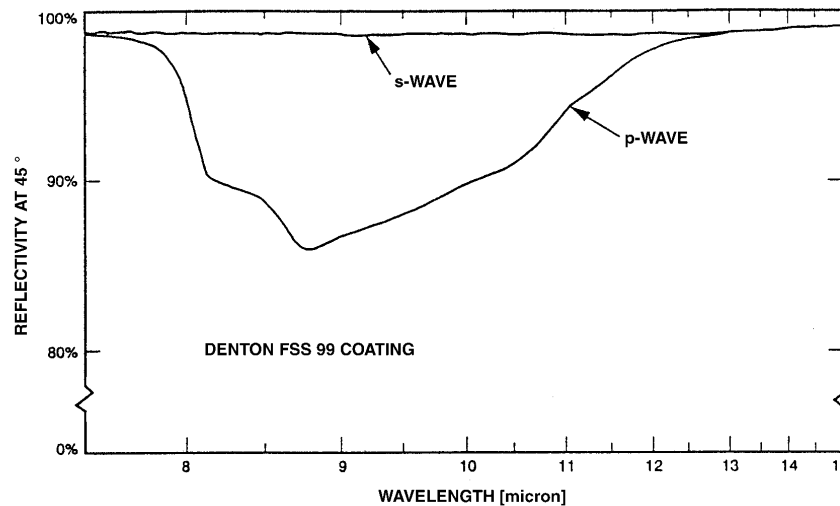
Figure 2.6

The spectral reflectivity for s- and p-waves between 7.5 and 15.5 μm (shown relative to the reflectivity of pure gold) introduces a scan angle dependent polarization effect with a peak-to-peak modulation of about four NeN units at 9 μm. The first order correction based on pre-launch characterization reduces the polarization effect to less than one NeN unit.

Let the scan mirror reflectance be r_p and r_s for the p- and s-polarizations. For an unpolarized incident flux, the polarization introduced in the flux on reflection from the scan mirror is

$$p_{scan} = \left| \frac{r_s - r_p}{r_s + r_p} \right| \qquad \text{Eq. 2-6}$$

If t_p and t_s are the transmissions parallel and perpendicular, respectively, to the plane of maximum polarization of the spectrometer, then define

$$p_t = \left| \frac{t_p - t_s}{t_p + t_s} \right| . \qquad \text{Eq. 2-7}$$

The plane of maximum polarization makes an angle α relative to the spectrometer x-z plane. The radiance emitted by the AIRS calibration source, N_c, is measured at mirror position $\delta = \pi$ and the space observation occur near $\delta = \pi/2$. We then express the true scene radiance, N_{true}, as the sum of the apparent scene radiance N, obtained from the basic calibration equation (Eq. 2-3) ignoring polarization effects, plus a correction term, dN_p, i.e.

$$N_{true} = N + dN_p, \qquad \text{Eq. 2-8}$$

where

$$dN_p = p_r p_t \left[N \left(\cos(2(\delta - \alpha)) - \left(1 - \frac{2N_s}{N_c} \right) \cos(2\alpha) \right) - N_s \left(\cos(2(\delta - \alpha)) - \cos(2\alpha) \right) \right] \text{Eq. 2-9}$$

N_s is the blackbody function of the scan mirror and δ is the rotation angle of the scan mirror about the x-axis. The angle of the spectrometer plane maximum polarization relative to the x-z plane, α, is wavelength dependent. The scan mirror temperature is measured in flight by a non-contacting temperature sensor built into the rotating axis of the scan mirror mounting assembly.

Figure 2.7 shows the magnitude of the correction, dN, due to the scan mirror polarization at 8.8 microns for scene brightness temperatures of 220 K (cloud tops), 285 K (clear ocean), and 320 K (desert) . At 8.8 microns we have r_s=0.98 and r_p=0.86, resulting in p_r=0.065. The estimated orientation of the grating relative to the scan mirror nadir position is α=22.5 degrees and the grating polarization based on theoretical predictions is p_t=0.25. For the 320 K brightness temperature, with a predicted signal of 800*NeN, the correction ranges from -14*NeN units at -49 degree scan angle to about +5*NeN units at +38 degree scan angle. For the 220 K brightness temperature, with a predicted signal of 78*NeN, the predicted correction ranges from -8*NeN units to -4*NeN units.
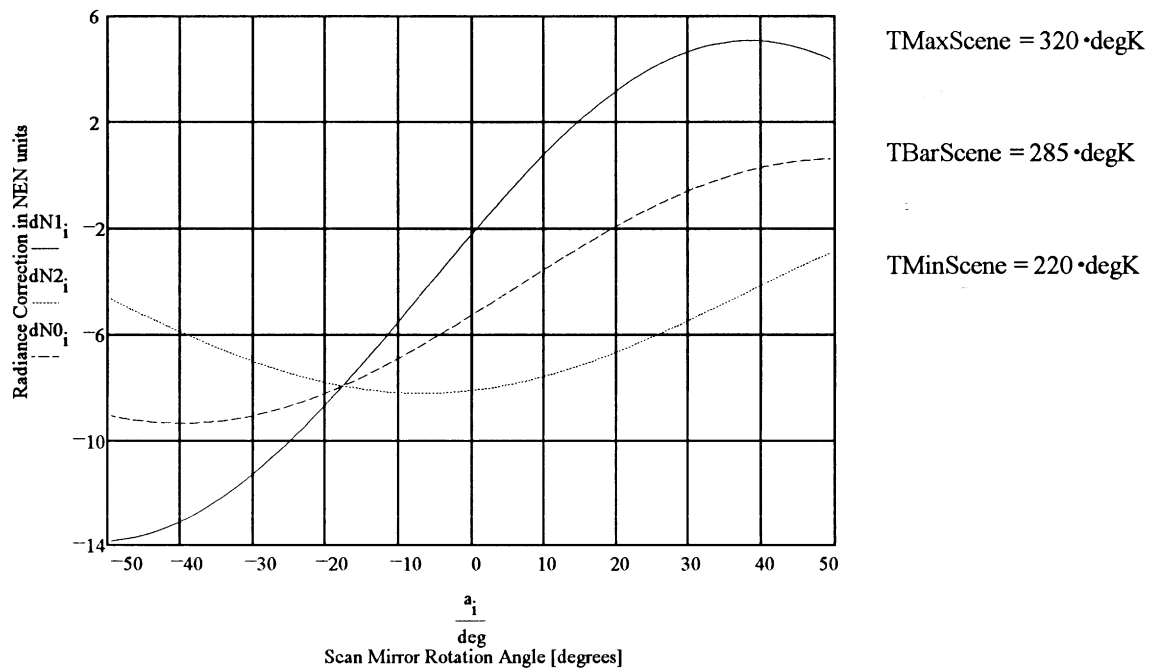
Figure 2.7

The correction, dN, due to the scan mirror polarization calculated for expected conditions at 8.8 microns and extreme scene brightness temperatures of 220 K and 320 K.

The polarization correction algorithm will be applied between 7.5 and 12 microns. The error estimates in Fig. 2.5 assume a nominal scene brightness temperature of 285 K, and a 5% residual after the polarization correction. Below 7.5 microns and above 12 microns scan mirror polarization effects are negligible compared to the NeN. This procedure will be validated during pre-launch characterization of the AIRS flight unit.

2.2.3.5 Residual electronics non-linearity

Residual electronics non-linearity is not expected to be a significant contributor to the radiometric error. The AIRS detector and electronics response to a signal covering the full dynamic range will be measured as part of the pre-launch characterization. The calibration algorithm removes electronics non-linearities using a combination of table lookup and polynomial fitting to create "linearized" or "rectified" data numbers. However, changes in the electronics due to aging and/or prolonged exposure to ionizing particle radiation in orbit (during the 5 year+ lifetime) may produce deviations from the pre-launch calibration. The magnitude of these residual non-linearities is difficult to estimate, but they could approach the calibration accuracy specified in the AIRS FRD for the 3.7 to 13.4 micron (HgCdTe:PV)

detectors. The AIRS electronics design therefore includes provision for a potential in-orbit re-calibration of the detector signal chain using a special calibration sequence. The dwell time for viewing the calibration blackbody can be changed in 1 ms steps from 1 ms to about 40 ms (the normal dwell time is 22 ms). This creates an extremely linear 40 step input signal to the electronics chain. The data from this sequence are used by off-line data processing on the ground to re-fit the electronics response. Residual non-linearities is not a concern for the 13.4 to 15.4 micron (HgCdTe:PC) detectors and electronics chain, but a similar sequence, with only eight steps between 2.75 and 22 ms, is available.

2.3 Spectral Calibration

The AIRS spectrometer has a nominal spectral resolution, $R \equiv \lambda/\Delta\lambda = 1200$. Figure 2.8 shows the AIRS Spectral Response Function (SRF) on a logarithmic scale in units of $\Delta\lambda$ from the centroid, where $\Delta\lambda$ is the full with at the half peak of the SRF. Depending on details of assumptions regarding optical blur and diffraction effects, the far wing response of the SRF rolls off as λ^{-2} to λ^{-3}. Either response is acceptable, as long as it is known with adequate accuracy. The AIRS FRD calls for knowledge of the wavelength of the centroid of each array element to within 1% of $\Delta\lambda$. Uncertainty in the knowledge of $\Delta\lambda$ is specified in the FRD to be no more than 1% of $\Delta\lambda$. In addition, the AIRS FRD limits the permissible drift of the centroid location to $0.05*\Delta\lambda$ during any 24 hour period. The centroid and SRF knowledge accuracy requirements were based on numerical experiments with climatologically representative radiance spectra. The infrared spectral calibration algorithm is based on the following strategy:

a) The AIRS spectrometer will be accurately calibrated pre-launch for a number of instrument conditions (temperature and optics alignment) centered on the expected in-orbit conditions. This includes the measurement of response centroids and SRF for each channel and the development of a focal plane model.

b) As the AIRS is equilibrating in orbit within the first month after launch, the ground-based spectral calibration algorithm will routinely determine the centroid of each channel. This is the "true wavelength" set, corresponding to the conditions within a 5 minute (TBD) smoothing window. Analysis of this data is expected to show that the wavelength of each channel drifts within $\pm 0.05 * \Delta\lambda$ around a mean wavelength. The set of mean wavelengths will be defined as the nominal AIRS channel set. The small wavelength shift has no effect on the SRF.

c) For routine operations the spectral calibration algorithm continues the monitoring of the "true wavelength" of each spectral sample. The calibration algorithm first determines the spectral radiances at the true wavelengths reported by the spectral calibration algorithm. It then creates the level 1b output by shifting the radiance spectrum from the true wavelength set to the standard AIRS wavelength set. The Level 2 retrieval algorithm is based on the standard AIRS wavelength set. Based on this strategy, the inflight spectral calibration consists of four algorithms:

1) A correlation algorithm for the analysis of selected regions of the upwelling spectral radiance (including a $1/20\ \Delta\lambda$ step upwelling spectral radiance file).

2) The focal plane model to extend the calibration to all detectors.

3) The regression algorithm to update the parameters of the focal plane model.

4) The algorithm to shift from current "true" wavelength to the standard wavelength set.

The theoretical basis of these algorithms is discussed in the following section.
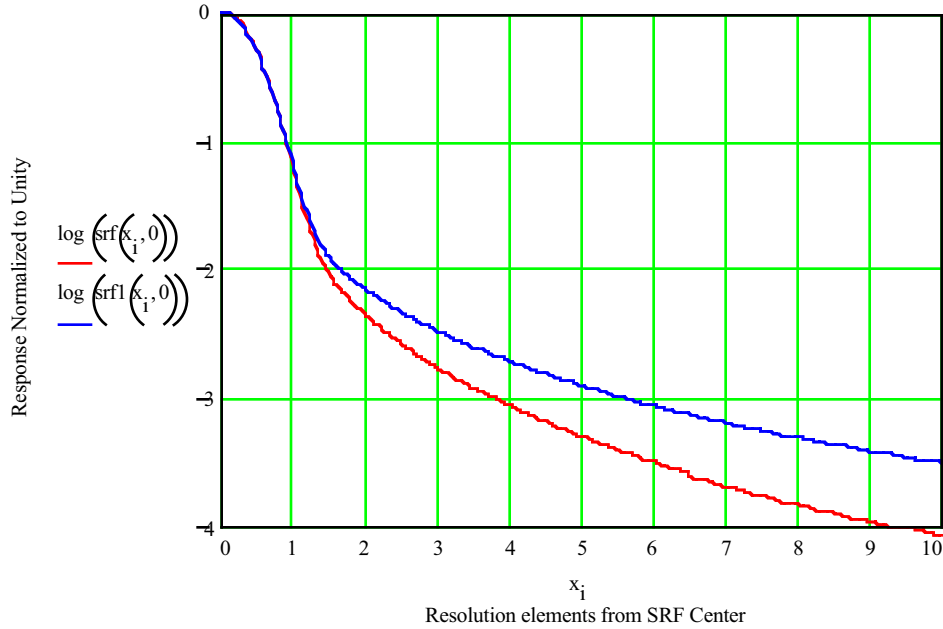
Figure 2.8

The AIRS Spectral Response Function (SRF) on a logarithmic scale in units of $\Delta\lambda$ from the centroid, where $\Delta\lambda$ is the full with at the half peak of the SRF normalized to unity. Depending on details of assumptions regarding optical blur and diffraction effects, the far wing response of the SRF rolls off as λ^{-2} to λ^{-3}.

2.3.1 Spectral Response Function Centroids (Wavelength Calibration)

AIRS achieves its absolute wavelength calibration by comparing the observed upwelling spectral radiance with the spectral radiance calculated numerically using knowledge of the line centers and strengths of active gases. The upwelling spectral radiance, which is observed on each detector in steps of $\Delta\lambda/2$, is compared using a correlation algorithm with the predicted spectral radiance calculated with step size $\Delta\lambda/20$. In principle, every AIRS spectrum could be used to check the wavelength calibration. In practice, four observations closest to nadir and under cloud-free conditions will be used for the routine monitoring of the spectral calibration. Recalibrations, if necessary, will be based on the analysis of about one hundred spectra gathered during five minute intervals.

The AIRS spectral calibration includes the application of a focal plane model. This model is derived from the grating equation

$$m * \lambda = d * (\sin \alpha + \sin \beta) \qquad \text{Eq. 2-10}$$

where m is the grating order, λ is the wavelength, d is the grating constant (the spacing between grating lines), α is the angle of incidence of light on the grating and β is the angle at which the diffracted light leaves the grating. In the case of AIRS, m ranges from 3 at the longest wavelengths to 11 at the shortest wavelengths. We can rewrite this equation to express the wavelength of detector i, λ_i, in terms of its position X_i in the direction of dispersion relative to a reference line X_o in the focal plane.

$$\lambda_i = \frac{d}{m} \left[\sin(\alpha) + \sin\left(a \tan\left(\frac{X_o - X_i}{L} \right) \right) \right] \qquad \text{Eq. 2-11}$$

where L is the distance of the focal plane from the focusing mirror. During the prelaunch alignment of the instrument L is set to an optimum distance (approximately equal to the on-axis focal length of the focusing mirror). L and X_o can be adjusted in-flight by turning three precision screws of the focusing mirror alignment assembly.

All detectors of an array are photo-etched on a common HgCdTe wafer and all arrays and associated readout electronics are mounted on a single ceramic substrate. The positions X_i of all detectors relative to X_o are measured when the focal plane is assembled and are verified during the spectral system calibration on the ground. Since the grating order m is selected for each array by order isolation filters, the wavelength calibration of the entire focal plane in flight depends on monitoring only four parameters: d, α, X_o and L. Changes in d, α, X_o and L after launch are all related to changes in the thermal environment and gravity release in orbit. Thermal environment changes occur in the vicinity of the poles as the spacecraft enters or leaves the Earth's shadow every 50 minutes. The response of the instrument to these changes is attenuated by the thermal inertia of the IR spectrometer. The thermal time constant of the spectrometer is estimated to be about 20 hours. Changes in the spectral calibration will therefore occur very slowly compared to the spectral calibration monitoring. We expect that almost the entire change in the spectral calibration after the initial stabilization period will be due to the temperature dependence of d, the grating constant, due to the temperature expansion coefficient of the grating material (Aluminum).

The basic concept of the AIRS wavelength calibration algorithm is as follows: we select small wavelength regions, each about 20 detectors wide, for each of the 17 arrays, and use the upwelling spectral radiance to solve for d, α, X_o and L with a regression algorithm (i.e. in a least-squares sense). The accuracy of this solution is in principle limited by uncertainty in the knowledge of the temperature and moisture profile and the finite signal-to-noise of the

detectors. In practice, a rough approximation of the temperature structure suffices to accomplish the spectral calibration. In most regions of the 3.7 - 15.4 µm spectrum, particularly near the edges of atmospheric window regions, the calculated spectrum based on the temperature and moisture profiles expected from climatology can be substituted for the true upwelling radiance spectrum. This is illustrated in Fig. 2.9. The Earth can be subdivided into rough climate zones: midlatitude/tropical, summer/winter, ocean/land. Each climate zone can be represented by a mean vertical profile and an extreme hot/cold/dry/wet profile. The climatology set with the largest difference between the mean and the extreme profile is the midlatitude/ winter/ ocean set. Figure 2.9 shows the spectral radiance calculated for mean and the extreme condition in the observed spectrum for the 693-736 cm^{-1} (13.59 - 14.39 µm) region of the spectrum calculated for the midlatitude/winter/ocean mean case and extreme case. This part of the spectrum is measured by the 144 detectors of focal plane module M-11 (Fig. 2.3). Now consider the 726-736 cm^{-1} region, which is at the edge of the CO_2 band. While the brightness temperature difference between the precalculated mean and the "observed" extreme case is about 20 K, the maxima and minima of the spectra are precisely aligned. This is because we picked a region with weak lines, not contaminated with underlying water lines, and because the AIRS spectral resolution is adequate to resolve the individual lines. A climatology based guess of the temperature profile is thus adequate for spectral calibration.

Although not all spectral regions covered by AIRS can be used for spectral calibration with as much ease as the 726-736 cm^{-1} example, there are enough regions to accomplish the least-square solution for the four key grating equation parameters discussed above. Finite signal-to-noise is the actual limit to the achievable spectral calibration accuracy. We indicated previously that we expect almost the entire change in the spectral calibration after the initial stabilization period to be due to a change in the grating constant, d, with temperature. This produces a shift $\delta\lambda = \Delta d * \lambda / d$ in the wavelength calibration. We use the 726-736 cm^{-1} region of the AIRS spectrum shown in Fig. 2.9 to illustrate that, with the AIRS nominal noise equivalent delta temperature, NEΔT, $\delta\lambda$ can be determined to satisfy the required spectral calibration accuracy with only four spectra.
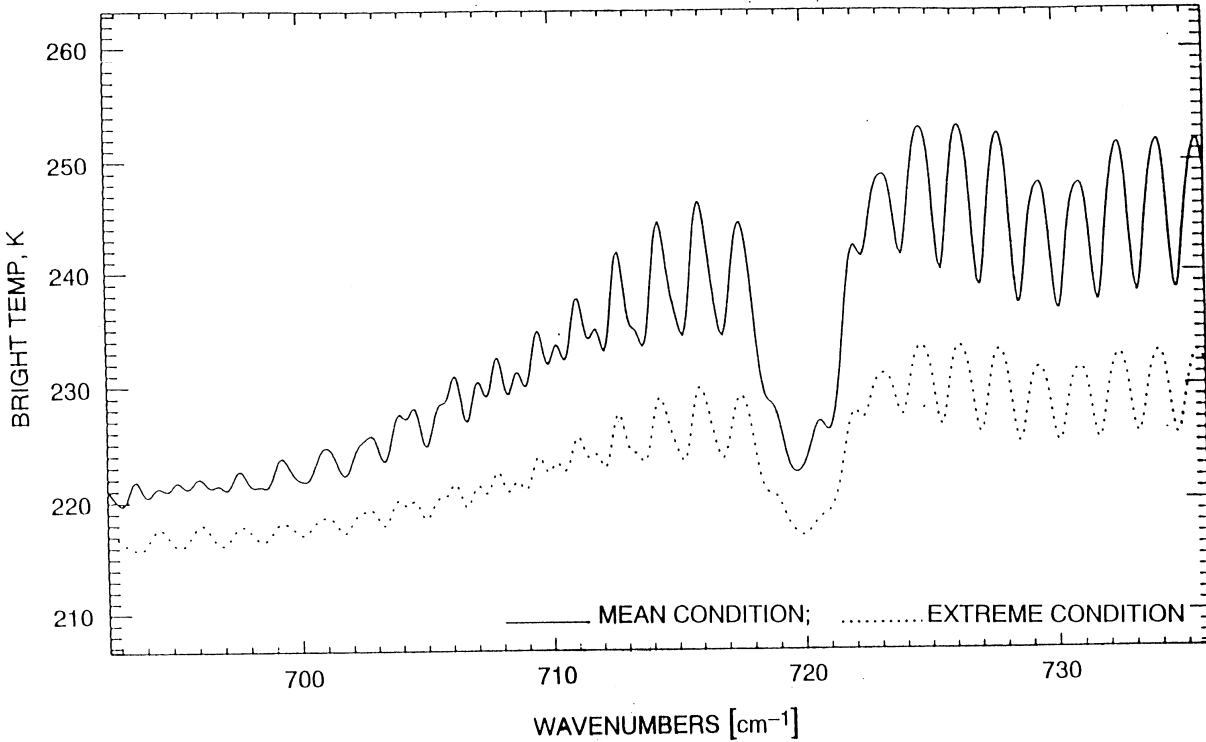
Figure 2.9

The upwelling radiance in the 692-736 cm⁻¹ region of the spectrum, shown here for the average and extreme winter/mid-latitude climatology, is measured by the 144 detectors of array M11. The spectrum illustrates that AIRS has enough spectral resolution to be "self-calibrating".

For conditions similar to those encountered in the 726- 736 cm⁻¹ region discussed above, the spectral calibration accuracy, $\delta\lambda$, is related to the spectral resolution width, $\Delta\lambda$, the peak-to-peak contrast in the signal, C, the rms noise of each detector element, NEΔT, and the number of detector elements, N, in the array. An approximate expression for the relation is

$$\delta\lambda = 2 * \mathrm{NE}\Delta\mathrm{T} * \frac{\Delta\lambda}{\mathrm{C}} * \sqrt{\frac{2}{\mathrm{N}}} .$$

Eq. 2-12

For the 726-736 cm⁻¹ region we have C = 12 K, NEΔT = 0.35 K, N = 18, resulting in $\delta\lambda$=0.02*$\Delta\lambda$. This accuracy is adequate for the routine monitoring of the calibration. Achieving the required wavelength calibration accuracy of 0.01*$\Delta\lambda$ requires in principle only four observations of the upwelling radiance. In practice, hundreds of upwelling spectra are available to monitor the accuracy of the spectral calibration and to apply corrections to the calibration, if necessary.

If the spectral contrast, C, is less than a 5 K (TBD) threshold, then the spectral calibration algorithm skips to the next AIRS footprint. Since the spectral calibration regions are selected specifically for high spectral contrast, the reason for low contrast is the presence of high clouds in all or part of the field-of-view. Clouds show very little spectral contrast in the infrared. To first order the spectral contrast in a partially cloudy scene decreases proportional to the fractional cloud cover. Figure 2.9 could thus be interpreted as representing mean climatology condition with a clear and a 50% cloudy field-of-view. Experience with TOVS data shows that 40% of the HIRS/2 footprints are infrared cloud-clear.

2.3.2 Standard AIRS Wavelength Set Shifting

The AIRS level 2 geophysical data retrieval algorithm expects level 1b data input at the standard AIRS wavelength set. Creating these spectral radiances is the last step in the level 1b algorithm. The shifting algorithm takes advantage of these facts:

a) The AIRS spectrum is sampled twice per resolution element.

b) The expected shift, $\Delta\lambda_i$, between the observed wavelength and the standard wavelengths is small; less than 5% of the FWHM of the SRF.

c) The shape of the spectrum is known and relatively insensitive to the climate condition.

At most wavelengths, a quadratic interpolation algorithm can be used to shift the wavelengths with negligible radiance error. At some wavelengths, some form of eigenfunction expansion is required. The coefficients of expansion will be precalculated and stored in a table. In its simplest form, the coefficients will be the mean first and second derivative (the mean from a globally representative temperature and humidity profile) evaluated at the standard wavelength. The shifted radiance set is then given by:

$$\mathbf{B}(\lambda_{is}) = \mathbf{B}(\lambda_{io}) + \left(\overline{\frac{d\mathbf{B}}{d\lambda}}\right)_i \Delta\lambda_i + \left(\overline{\frac{d^2\mathbf{B}}{d\lambda^2}}\right)_i \frac{\Delta\lambda_i^{\,2}}{2} \qquad \text{Eq. 2-13}$$

2.3.3 Spectral Response Function Width

Accurate knowledge of the SRF width is second in importance only to knowledge of the SRF centroid for the accurate calculation of the transmittance function. Errors in the knowledge of the SRF will mimic spectroscopic errors, which, under some conditions, may exceed several times the NeN. The AIRS spectrometer SRF shape and centroid (for each detector) is measured prelaunch using an FTS spectrometer (Brucker Model 65) over a wide range of spectrometer parameter conditions centered on the conditions expected in orbit. AIRS contains no means of directly measuring the SRF width onboard, but the level 1b algorithm routinely solves for parameters related to the SRF and, if necessary, for setting an alignment device by ground command.

The full width of the AIRS SRF, $\Delta\lambda$, is determined by the convolution of four elements:

a) The spectrometer entrance slit, essentially a rectangular hole cut in an Aluminum mask.

b) The spectrometer exit slit. The area of each detector acts as the exit slit in an array spectrometer.

c) The grating diffraction response function, and

d) The optical point spread function (PSF) of the spectrometer optics. The PSF is given by the convolution of the geometrical image blur, diffraction blur and out-of-focus blur.

The first three of these components, which determine the SRF to first order, are fixed. Changes in the PSF produce a second order broadening effect on $\Delta\lambda$. This effect can be detected and eliminated in-orbit. In the previous section we expressed the wavelength of detector i, λ_i, in terms of its position X_i in the direction of dispersion relative to an arbitrary reference line X_o in the focal plane. During the prelaunch alignment of the instrument, L is set equal to the focal length of the focusing mirror. Vibration during launch, unforeseen thermal disturbances or material creep during 5 years in orbit may shift L and/or X_o away from the position for which the SRF's were measured during pre-launch characterization. Since L and X_o are determined for the entire focal plane as part of the routine spectral wavelength calibration monitoring, a shift from the pre-launch value X_o in combination with a change in L is indicative of a focus change. Both L and X_o can be readjusted in-flight to their pre-launch values by turning three precision screws of the focusing mirror alignment assembly.

2.4 Spatial Calibration

The AIRS infrared data, with a 1.1 degree FOV, will be analyzed simultaneously with microwave data from the AMSU (3.3 degree beam), and the HSB (1.1 degree beam). Knowledge of AIRS FOV location on the ground has to be within a 255 arcsec half cone angle. The requirement is easily met by the spacecraft knowledge of the pointing vector within 12.2 arcsec (1 sigma). The selection of several AIRS FOV within the AMSU FOV is thus based on the data from the instrument integration. Details of the selection of FOV clusters located within the AMSU FOV are discussed in the level 2 ATBD. No AIRS infrared pixel interpolation is included in the level 1b algorithm.

2.4.1 Infrared Boresight Validation

Validation of the AIRS infrared boresight is planned at the team leader facility to facilitate cross-comparisons between AIRS and other instruments on the EOS PM spacecraft. The algorithm will make use of the statistics of crossings of high contrast scenes (e.g. transitions from land to ocean) to determine a longitude and latitude offset angle between the apparent boundary location and the true boundary location. If the temperature contrast between ocean

and land is DT_{ol} , the spectrometer noise equivalent temperature per footprint is NEΔT, the angular footprint diameter is Φ, and the average angle between the cross-track scan and the coastline intersection is α, then the statistical accuracy of the cross-track position accuracy determination from n crossings is

$$\frac{D\Phi(n)}{\Phi} = \frac{NE\Delta T \cos(\alpha)}{DT_{ol}\sqrt{n}}$$

Eq. 2-14

For typical values of α=45 degree, NEΔT=0.2 K and DT_{ol}=10 K, we obtain

$$\frac{D\Phi(n)}{\Phi} = \frac{0.03}{\sqrt{n}}.$$

Cross-track boresight determination (as the difference between the infrared boresight observed and the geometric boresight calculated) to within 1% of the AIRS field-of-view is achievable with 10 coastline crossings. In practice, a single orbital pass along the Baja California produces about 200 coastal crossings suitable for verification of the infrared boresight. This scheme has been used successfully on ERBE and will be also be used on CERES on the EOS AM spacecraft.

2.4.2 Measurement Simultaneity.

The AIRS data analysis assumes that the spectral radiances produced by the level 1b algorithm correspond to a single "footprint" on the ground at all wavelengths. This spatial concurrence of all wavelengths is referred to in the AIRS FRD as the "Cij" requirement. C_{ij} is a measure of the alignment of the centroid of the i-th spectral channel relative to the j-th channel as a fraction of the beam diameter. The FRD specifies $C_{ij} > 0.99$ for all channels, i.e., the beam centroids of all wavelengths are aligned to within 1% of the beam diameter. This requirement is identical to the requirement imposed on the HIRS/2 on NOAA K. Previous HIRS/2 instruments have typically achieved $0.9 < Cij < 0.95$. The single entrance aperture design of AIRS insures meeting the C_{ij} requirement to first order. No algorithms are envisioned to measure C_{ij} in orbit or to adjust or improve spatial alignment of the infrared channels relative to each other using pixel interpolation.

2.5 AIRS Infrared Radiometric Calibration Algorithm

In the following we describe the steps which will be taken to perform the radiometric calibration of the AIRS instrument. We assume that the AIRS spectrometer meets the specification described in the AIRS Functional Requirements Document (Ref. 2).

The first data regarding the spectrometer thermal stability, spectral resolution, wavelength stability, electronics linearity and detector noise will come from the engineering model tests in

the summer of 1997. Scan mirror measurements (emissivity, temperature and temperature gradient) will become available in the summer 1998 during the characterization of the AIRS flight model. All changes in the state of the spectrometer, such as gain changes, switching to backup electronics modules etc., which will cause a discontinuity in the calibration, are assumed to be available as a listing of the ground command or as a command verification echo from the instrument. This eliminates significant complications in analyzing calibration trends and results in a relatively straight forward calibration parameter smoothing algorithm design.

Revisions or refinements to the calibration algorithms based on the test results will be incorporated into updated editions of the Level 1b ATBD.

2.5.1 Dataflow Description

Figure 2.10 shows a top-level diagram of the AIRS IR radiometric calibration dataflow, from level-1A engineering units (and ancillary data) through level-1B calibrated preliminary (not spectrally corrected) radiances. The steps can be summarized as follows:

a) Use space views to determine DC Restore (DCR) discontinuities.

b) Use space views and calculated DCR discontinuities to determine detector offsets.

c) Use blackbody views and calculated detector offsets to determine detector gain.

d) Use scene radiances and calculated detector offsets and gain to produce calibrated radiances.

2.5.2 Preliminary Processing Corrections

Some processing steps are performed on each and every data number (this includes scene views, space views, and blackbody views). Because these steps can be applied directly to the input data numbers (before beginning the offset and gain calculations) they are grouped together here as pre-processing corrections. At present the only correction which will be done this way is the linearity correction.
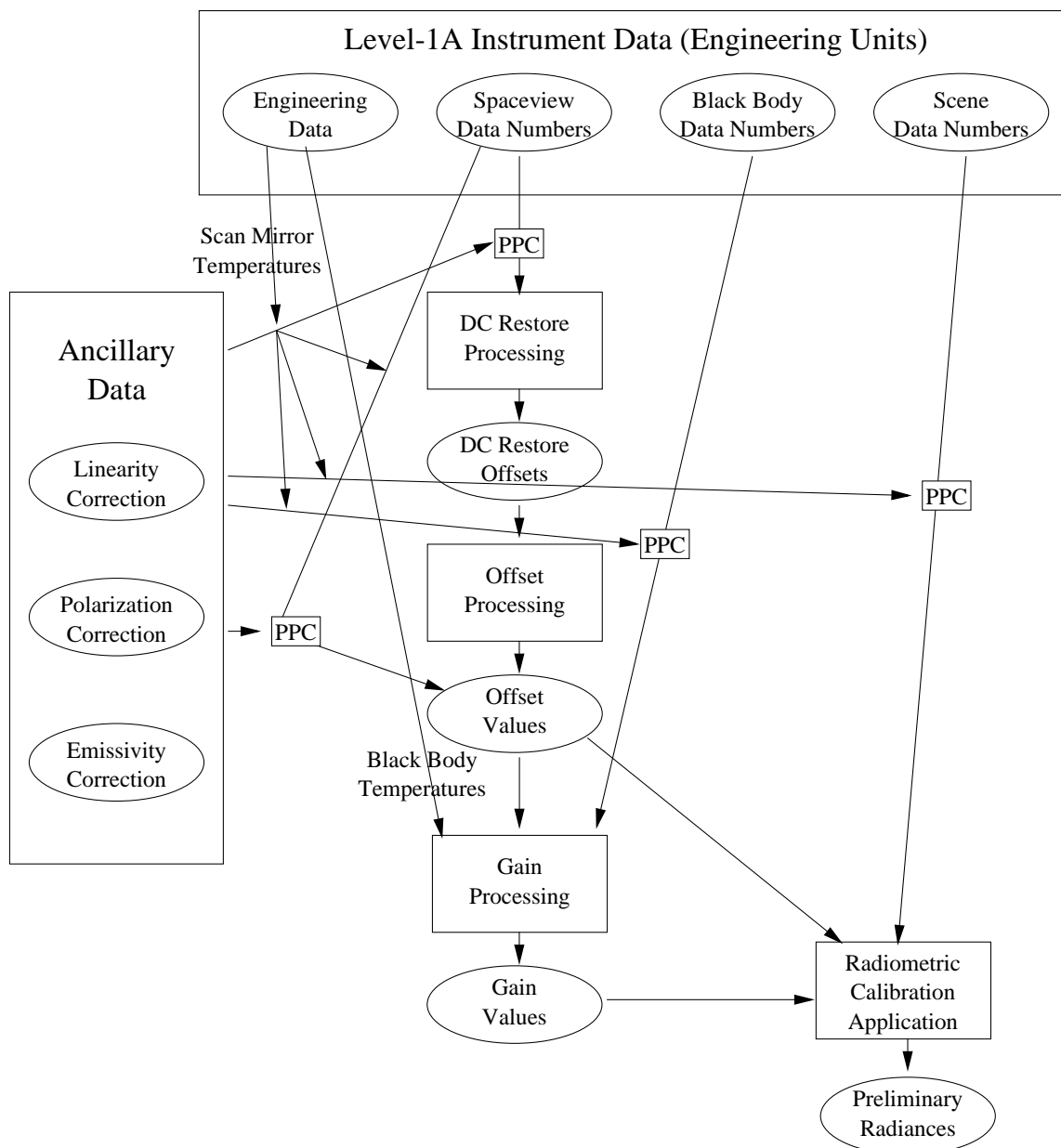
Figure 2.10

Top-level diagram of the AIRS IR radiometric calibration dataflow, from level-1A engineering units through level-1B calibrated preliminary (not spectrally corrected) radiances.

2.5.2.1 Linearity Correction

Prior to being used for processing, footprint data numbers (including scene views, space views, and gain views) are corrected for non-linearity. This consists of using a pre-calculated look-up table (probably generated from a polynomial) to adjust observed counts to a linearized output. The linearized counts are referred to as "rectified counts". The data for this transformation come from pre-flight measurements, and may be updated based on in-orbit linearity assessments.

2.5.3 DC Restore Processing

The magnitude of the discontinuity in each of the DC restored channels must be determined each time such discontinuities occurs. Suitable space views are used to assess these discontinuities.

2.5.3.1 DCR Space View Selection

Not all space views are suitable for use as reference points for monitoring detector offset levels. Currently two problems are expected which would make space views unsuitable: contamination from the moon, and contamination from the Earth's limb.

Using geolocation tags and ephemeris data, determining the angular separation between the moon (or the Earth's limb) and the instrument's field of view is straightforward. Those space views which are deemed to be an adequate angular distance from both the moon and the Earth are the only ones used. Desired separations will be determined during the in-orbit check out period.

2.5.3.2 DCR Fitting

Once suitable offset views have been identified for some duration on either side of a DC restore (perhaps five minutes; this will be determined during the pre-flight testing and/or the in-orbit check out period), a function of counts versus time will be fit separately to each side of the discontinuity. Alternatively, a slope-matching criterion may be added. By evaluating each of the two resulting functions at the time of the DC restore, the discontinuity is observed and quantified (see Fig. 2.11). The form of the function to fit will be determined during the pre-flight testing and/or the in-orbit check out period (and will probably be a quadratic or cubic polynomial). By adding the observed offset to the offset up to that time (for each channel), a cumulative DCR offset is calculated. This allows for reconstruction of a continuous data set, for as long as the instrument remains powered.

DCR Offset

Counts
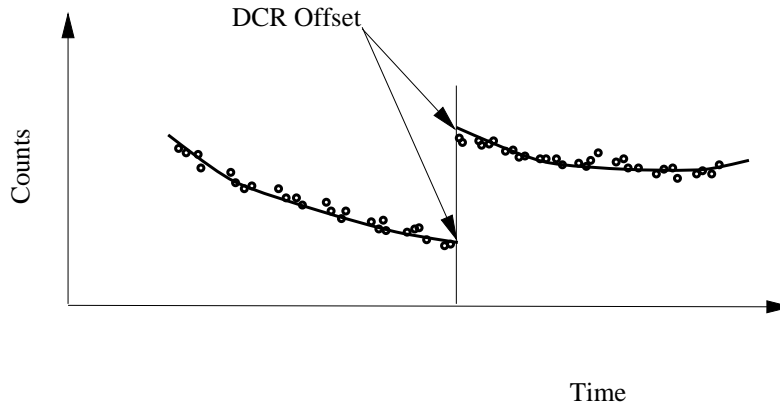
Time

Figure 2.11

By fitting the space views from before and after the discontinuity at the time of the DC restore, the discontinuity step can be quantified and used in the spaceview smoothing procedure.

2.5.4 Offset Processing

Pre-processed space views are used, for each channel, to determine the instrument response to a zero-radiance scene. This response is in units of counts (dn).

2.5.4.1 Offset Space View Selection

The selection criteria for space views for offset processing are identical to the criteria for space view selection for DC Restore processing. See Section 2.5.3.1 for additional details.

2.5.4.2 Offset Fitting

Because there is measurement noise on the space views, it is desirable to combine many space views, thereby obtaining a $\sqrt{N}$ decrease in noise levels. (Beyond about five minutes, however, 1/f noise begins to dominate and further combination of space views start to degrade the measurement accuracy.) Because the offset level in each detector may change with time, it is desirable to fit to the smoothed variation in observed space view counts, rather than simply taking an average.

2.5.4.3 Sliding Window Approach

Because we can assume that the true offset (and gain) of a detector at a given instant is reflected by measurements made close to that time, and because offset is subject to variation,

it is clear that the best determination of instantaneous offset is made when the set of space views which are being fitted to are centered on the time of interest (assuming no data drop-outs).

By making this fitting "window" large (about five minutes), not only is the noise reduced, but a smoothing operation is also performed. Specifically, this approach can be expected to reduce the point-to-point variability of calculated offsets by as much as a factor of 10 (there being some 120 scan sets in five minutes).

2.5.5 Gain Processing

Pre-processed blackbody views are combined with calculated offset values and blackbody temperature measurements to determine each detector's gain.

2.5.5.1 Gain View Selection

Blackbody views for which temperatures have been measured are selected (these should be all the blackbody footprints). In the absence of blackbody temperatures (e.g., if the engineering data packet is missing) no gain calculation can be done.

2.5.5.2 Blackbody Radiance Calculation

For each spectral channel, blackbody (Planck) radiances, $N(i)$, are calculated using the effective blackbody temperature, $T_e(i)$. The effective blackbody temperature is based on the weighted mean of the four measured blackbody temperatures (see Section 2.2.2). The weights are determined prior to launch. Due to slightly different viewing geometries each detector will have its own set of weights.

2.5.5.3 Instantaneous Gain Calculation

If the detector electronics measures count V_c when viewing the internal blackbody with radiance N_c, and V_s when viewing cold space, the instantaneous detector gain

$$G = \frac{N_c}{V_c - V_s} \qquad \text{Eq. 2-15}$$

in mW / m^2 cm^{-1} sr / count.

2.5.5.4 Gain Fitting

Because there is noise on the gain calibration views, it is desirable to combine (N) gain views, thereby obtaining a $\sqrt{N}$ decrease in noise levels. (This is true up to a point. Beyond about five minutes, 1/f noise begins to dominate.) Because the gain of each detector (or its

electronics chain) may change with time, it is desirable to fit to the smoothed variation in observed gain, rather than simply taking an average of blackbody views and space views.

2.5.5.5 Sliding Window Approach

The approach taken for smoothing gain values over a sliding window is identical to the approach taken for smoothing offset values. See Section 2.5.4.3 for additional information.

2.5.6 Radiometric Calibration Application

2.5.6.1 Two point calibration

Given the calculated offsets and gains, calibrated radiances are obtained directly by subtracting the calculated offsets from the pre-processed observed scene counts, and multiplying this difference by the calculated instrument gain. The radiance emitted by a blackbody source is given by:

$$N_c = \frac{1.1911 * 10^{-5} * \nu^3}{e^{1.4388\frac{\nu}{T_e}} - 1}$$

Eq. 2-16

in units of mW/m^2 cm^{-1} sr, where T_e is the effective blackbody temperature and ν is the channel centroid frequency in units of wavenumbers (cm^{-1}). The wavenumber, ν , is related to wavelength, λ, (in μm) by:

$$\nu = \frac{10^4}{\lambda} \ .$$

Eq. 2-17

(The units are selected to maintain compatibility with NOAA.)

2.5.6.2 Polarization and Angle-dependent Scan Mirror Emission Correction

Because there is a polarization-dependent component of scan mirror reflectivity in the 7.5 - 12.5 micron range, and because the polarization vector rotates with the rotation of the scan mirror, it is necessary to introduce a polarization correction over this spectral range as discussed in Section 2.2.3.4. The correction is given by

$$N_{true} = N_t + dN(\theta)$$

Eq. 2-18

where N_t is calculated using the smoothed gain and space view and dN is given in Section 2.2.3.4.

2.6 Spectral Calibration Software

The process discussed in Section 2.5 produces preliminary radiances at the true (i.e., currently valid) spectral wavelengths set. The standard wavelength for each detector is used in the evaluation of the Planck function. The true wavelength set differs from the standard wavelength set by as much as $0.05*\Delta\lambda$. This is sufficiently accurate for the radiometric calibration when viewing a spectrally contrast free target. When viewing a high spectral contrast target, such as the upwelling spectral radiance, a more accurate wavelength calibration and a small correction to the radiometric calibration is needed.

Spectral features in cloud-free upwelling (near-nadir) radiances are used to determine the spectral characteristics of the instrument, including detector band centers and band widths. Figure 2.12 illustrates the dataflow for this process.

2.6.1 Spectral Feature Identification

Prior to launch, a number of small spectral regions (such as the 726-736 cm^{-1} region in Fig 2.9) are identified, to be fitted to for the spectral calibration. These spectral regions are chosen based on climatology and atmospheric model results, and must satisfy the following criteria:

a) The band centers of the features must not change in wavelength, over the range of atmospheric conditions (except cloudiness) expected.

b) The features chosen must provide good spatial coverage of the focal plane, preferably with one or more features in each of the detector arrays.

c) The features chosen must be located far enough from the ends of the detector arrays in which they fall, so that the fit of each spectral feature does not span detector arrays.

2.6.2 Clear View Identification

In orbit, cloud-free views (or nearly cloud-free views) are best for spectral calibration. Spectral calibration requires identifying which (if any) of the four footprints in each scan-line nearest the nadir are cloud free. This is accomplished using contrast thresholds.

2.6.3 Observed Spectral Position (SRF Centroid) Determination

A fit is performed for each spectral feature, determining the position of the center of that feature, in microns, relative to the beginning of the detector array in which it falls. This will probably be accomplished by relying on maximizing the correlation with an over-sampled synthetic spectrum of the same feature. It also relies on knowledge of the detector spacing within each detector array.
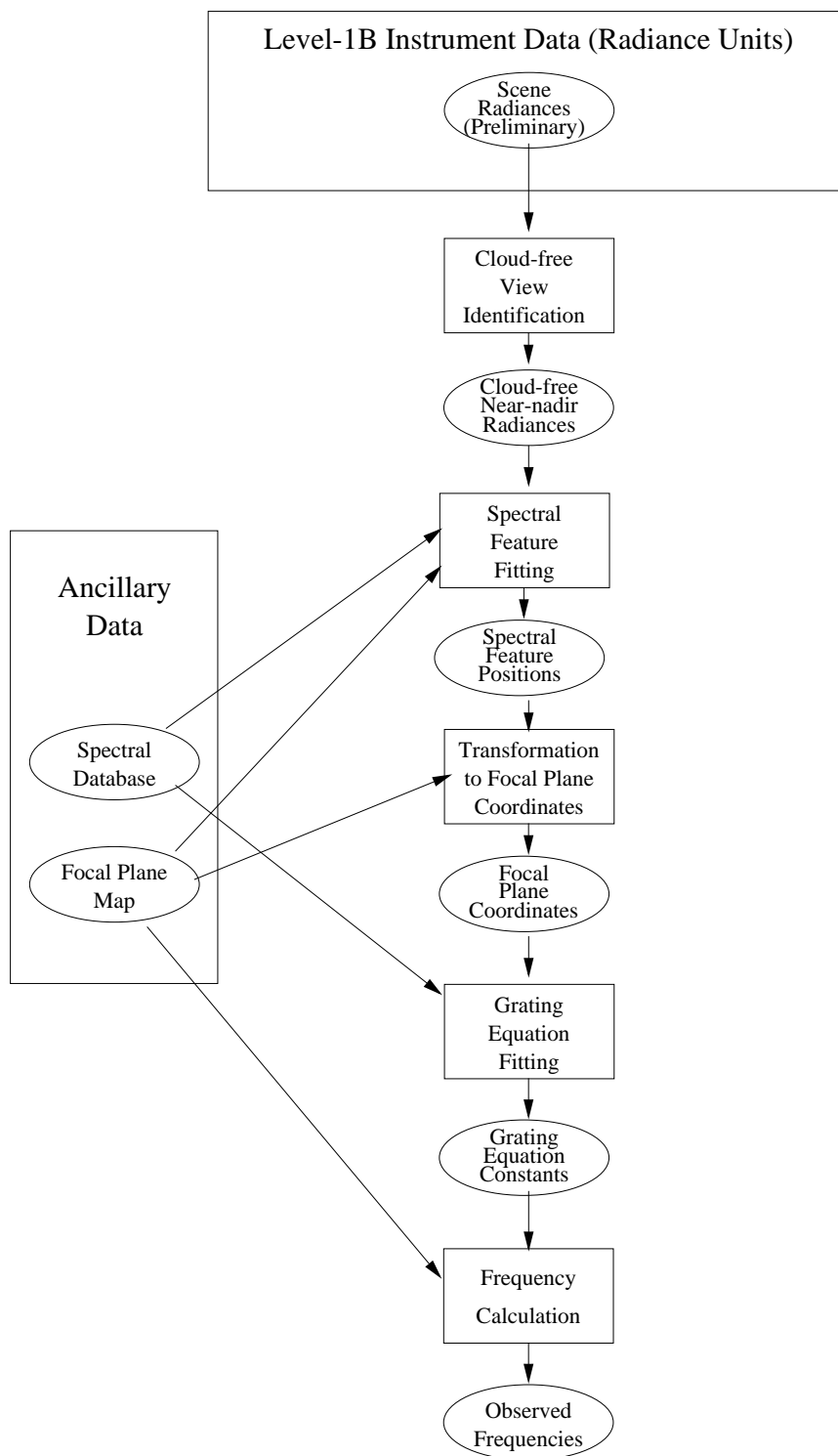
Figure 2.12

The dataflow for the spectral calibration.

2.6.4 Conversion to Focal Plane Coordinates

Relying on the instrument focal plane map (measured pre-launch, and assumed to be invariant during the mission), the observed positions of the spectral features in each detector array (in microns) are converted to positions (again in microns) on the focal plane relative to the X_o reference axis. This is accomplished simply by adding (or subtracting), for each spectral feature, the position (relative to the focal plane nominal axis) of the beginning of the detector array within which that spectral feature falls to the position of the spectral feature within the array.

2.6.5 Spectrometer Constants Determination

By inserting the observed positions (in microns) of the spectral features into the spectrometer grating equation (Eq. 2-11) using estimated values for the grating equation constants (d, α, X_o and L), a set of approximate resultant $\lambda(i)$'s are calculated, one for each spectral feature fitted to. Comparing these wavelengths with the known, true wavelengths of the spectral features provides us with a least-squares metric with which to assess the quality of the estimated grating equation constants. These "constants" are modified, using a simple hill climbing method and/or a more complicated global maximum location scheme, as needed, until best-fit values have been determined.

2.6.6 Detector Centroid Calculation

Using the calculated grating equation constants, and the known positions of each detector element on the focal plane (from the focal plane map), the observed positions of the detectors are produced directly from the grating equation.

2.6.7 Final Radiometric Calibration

The preliminary spectral radiances are shifted from the true wavelength set to the standard wavelength set using a 5 point interpolation formula.

2.7 Quality Control/Error Estimates/Exception Handling

2.7.1 Quality Control

Quality control of level-1B products is achieved primarily by analysis of the level-2 products which are produced from them. "Tuning" (see Section 2.2.4 and the level-2 ATBD) is the method by which the quality of the level-1B products is ensured.

2.7.2 Error Estimates

Uncertainties in the level-1B products (offsets, gains, and radiances) are quantified based on two primary indicators. The first of these is the quality of the fits that are done to offset and

gain. These quality indicators are in the form of correlation coefficients. The second quality indicator is the availability of calibration data. If many spaceview footprints are missing over the desired five minute interval, we know that the noise level will be higher. This concept will be developed quantitatively using experience gained with the engineering model.

2.7.3 Exception Handling

Because the level-1A processing will have analyzed the quality of the instrument telemetry (testing for completeness and corruption), no garbled data should be processed. The only exception currently anticipated is the possibility of data drop-outs (gaps), and the impact of these on level-1B processing is minimal. If scene footprints are missing, they are simply not calibrated. If calibration footprints are missing, there should be plenty of others within the five minute window with which to work. The only exception for which actual handling is done is the ability to begin and end processing smoothly when gaps longer than five minutes are encountered. Other exceptions (notably spurious data) can be handled in the footprint selection routines (see Sections 2.5.3.1, 2.5.4.1, and 2.5.5.1) as required.

2.8 References

1. H. H. Aumann and Chris Miller "Atmospheric Infrared Sounder (AIRS) on the EOS Observing System". SPIE Vol. 2583, 332-343 (1995).

2. AIRS Functional Requirements Document, JPL Internal Document D- 8236, Rev. 1., Oct. 1992.

3. World Meteorological Organization, "The World Weather Watch Programme 1988-1997", WMO-No. 691 (1987)

4. L. D. Kaplan, Inference of atmospheric structures from satellite remote radiation measurements, J. Opt. Soc. Am., Vol. 49, 1004-2007 (1959).

3. AIRS Visible/Near-Infrared Channels

3.1 Introduction

The AIRS instrument includes four visible/near-infrared channels, in the following discussion referred to as visible channels, with output in units of W/m^2. The discussion of the algorithms necessary to support the science objectives of the AIRS visible channels requires a brief description of the hardware implementation. The visible channels are implemented with four linear arrays, each array having nine pixels. Each pixel has a rectangular field-of-view 1/6 the size of the AIRS infrared 1.1 degree diameter footprint. The cross-track scanning is accomplished with the scan mirror in common with the infrared spectrometer (Section 2). Figure 3.1 shows the optical schematic of the visible channels.
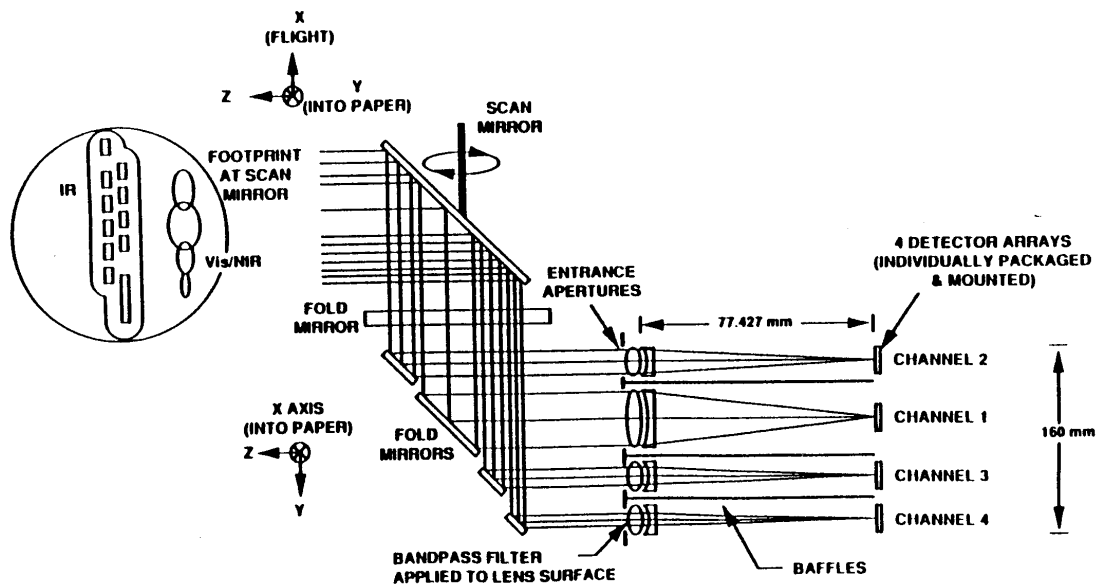
Figure 3.1

Optical schematic of the visible channels. Unlike the field of view of all infrared channels, which is defined by a single field stop, the fields of view of the visible channels are defined by the locations of the four arrays in the image planes of the four entrance apertures.

Unlike the field of view of all infrared channels, which is defined by a single field stop, the fields of view of the visible channels are defined by the locations of the four arrays in the image planes of the entrance apertures. Figure 3.2 is a schematic of the detector layout. Throughout this section, the term "visible pixel" is used to describe a square region on a detector, 250 μm by 250 μm. Each pixel, however, is composed of 10 sub-elements, a sub-

element being 250 μm in the scan direction, $\hat{y}$, but only 25 μm along the array axis, $\hat{x}$. As originally envisioned, only one sub-element of each pixel would be sampled, leaving 90% of a pixel's area unobserved. Consideration is currently being given to sampling all elements to provide complete coverage.
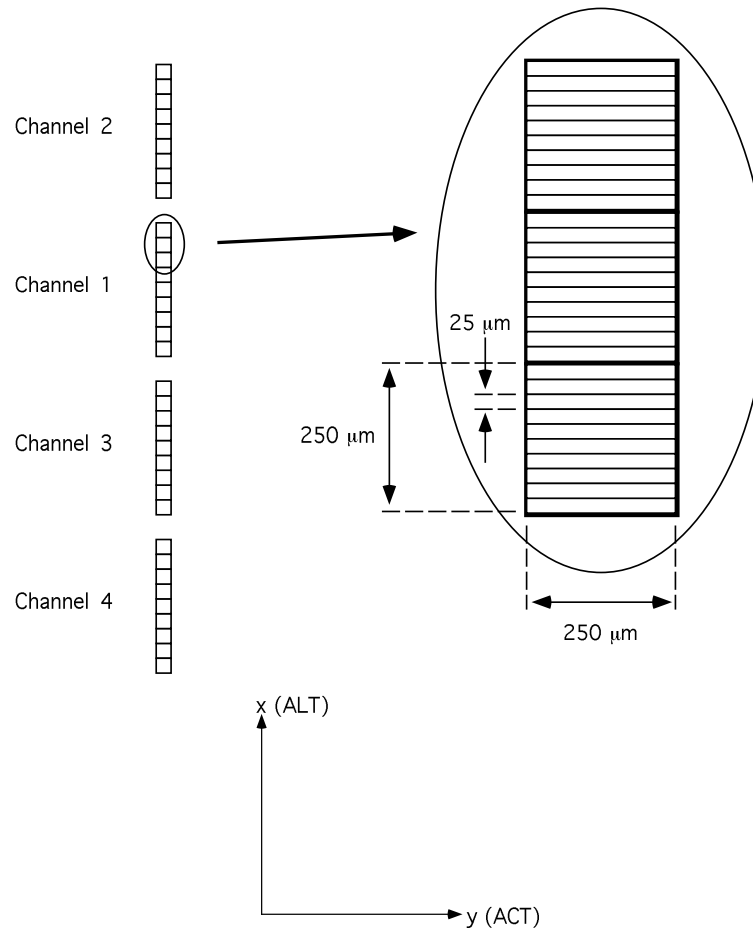
Figure 3.2

Schematic diagram of the layout of visible detectors within the AIRS instrument. Each pixel is 250 μm on a side, and is composed of 10 sub-elements. Each sub-element is 25 x 250 μm. Each detector array is aligned to within 0.001 radians of the instrument x-axis (the instrument scans along the y-axis). Note that the x and y axes correspond to the spacecraft's along-track (ALT) and across-track (ACT) directions, respectively.

The four detector arrays are aligned pre-launch to within 25 microns parallel and perpendicular to the crosstrack scan direction. The actual fields of view and positions of the visible detectors relative to each other and relative to the centroid of the infrared footprint will be determined during pre-launch characterization. Verification and monitoring of the spatial

alignment of the visible detector footprints relative to each other and relative the infrared footprint is carried out in orbit. Procedures and algorithms for the mapping of the visible channels relative to each other and relative to the infrared footprint is discussed in Section 3.4. Figure 3.3 shows schematically the ground location of the visible footprints relative to the circular spectrometer footprints near nadir for three scan lines from a 705 km orbital altitude. The size of a visible pixel on the ground under these conditions is 2.256 km, while the infrared footprint diameter is 13.54 km.
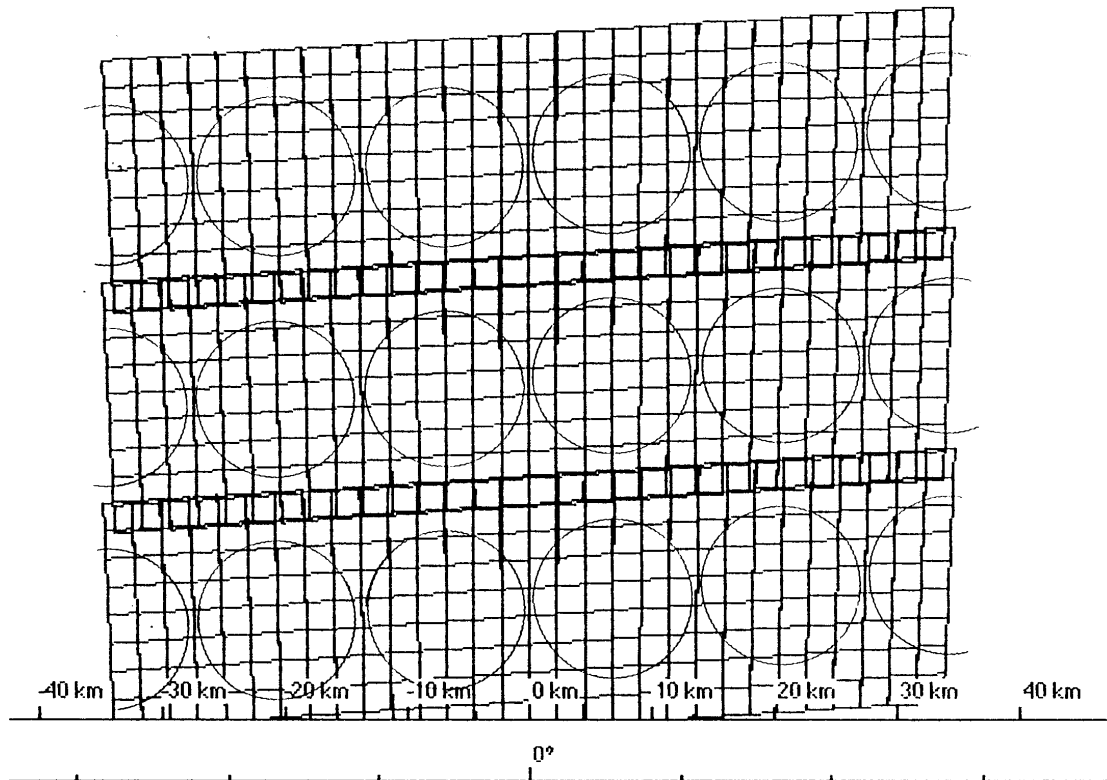
Figure 3.3

Schematic of the ground location of the visible footprints relative to the circular spectrometer footprint near nadir for three scan lines from a 705 km orbital altitude.

The primary purpose of the visible channels is to provide diagnostic capability in the presence of low clouds for the temperature retrieval (using the infrared channels). The data are typically analyzed as ratios R_i/R_j or $(R_i-R_j)/(R_i+R_j)$, or R_i/I_j, where I_j is the solar reflected radiance from some channel between 3.7 and 4.1 microns. For this purpose we need

- accurate spatial alignment between the AIRS visible and infrared footprints, to create infrared equivalent visible footprints. For this purpose knowledge of the pixel centroids to about half the pixel diameter, i.e. 1.1 km or 5.5 arcmin is adequate.

- stable relative (photometric) response, since the quality indicators are empirically determined. This requirement is consistent with the hardware, which supports stable photometric response, but the pre-launch absolute calibration accuracy is good to only 20%.

The secondary purpose of the visible channels is to support research products related to the AIRS core data product (temperature and moisture sounding). Such research products include downwelling short-wave radiation and determination of the height of low clouds. For this purpose we need good relative photometric accuracy and radiometric calibration with about 5%-10% absolute accuracy. This requirement is not supported by the hardware implementation, but can be reached through vicarious calibration and cross-calibration with other instruments, in particular MODIS. This is discussed in Section 3.2.4. Simultaneous analysis of MODIS and AIRS data under normal scene contrast conditions would require knowledge of the pixel centroids to about half the diameter of the MODIS pixels, i.e. between 0.125 and 0.5 km or 0.6-0.24 arcmin for the visible channels. This requirement can be considerably relaxed under the low scene contrast conditions typically selected for cross-calibration.

The spectral response curve of the visible channels is defined by the product of the spectral response of four elements:

a) Sharp cut-on and cut-off interference filters (except for a long pass filter in channel 4, which uses a longwave pass-filter).

b) The optics reflectivity (3 reflections, including the scan mirror).

c) The transmission characteristics of the field imaging lenses, and

d) The spectral response curve of the Silicon detectors.

The nominal transmission characteristics of the VIS/NIR channels are as follows:

Channel Number	50% Cut-on [microns]	50% Cut-off [microns]	2% Cut-on	2% Cut-off
1	0.40 +/- 0.005	0.44 +/- 0.005	>= 0.38	<=0.46
2	0.58 +/- 0.02	0.68 +/- 0.02	>= 0.55	<=0.71
3	0.71 +/- 0.02	0.95 +/- 0.02	>= 0.67	<=1.02
4	Note 1	1.0 (Note 2)	>= 0.35	1.1 (Note 2)

Note 1. More than 25% at 0.4 microns, more than 50% response at 0.45 microns.

Note 2. Long wavelength spectral extent of channel 4 is defined by the radiation dose dependent cutoff wavelength of the Si diode.

The scan mirror and the folding mirrors of the optics are Silver coated with a thin layer of SiO_x, using Denton proprietary process FSS99. The reflectivity of this coating is 99%, with no polarization dependence (in the 0.4 to 1.1 µm region).

Figure 3.4 shows the preliminary spectral response functions of the four channels based on the vendor supplied transmission and spectral response characteristics of the subsystem components. The final response curves will be delivered as part of the instrument characterization record.
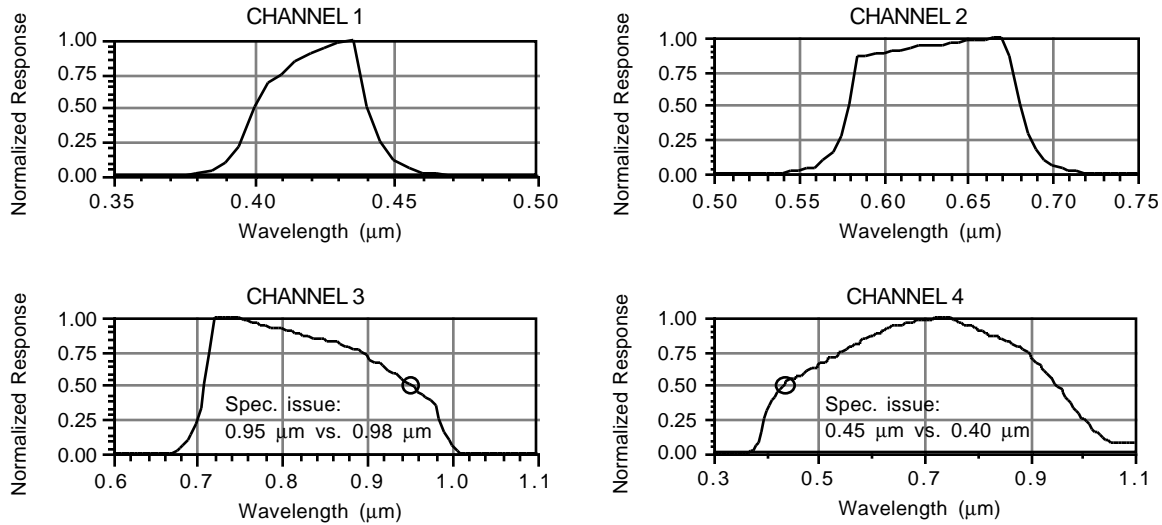
Figure 3.4

The preliminary spectral response functions of the four channels.

The long wavelength spectral extent of channel 4 is defined by the radiation dose dependent cutoff wavelength of the Si diode. Figure 3.5 shows the relative response of the Si diode before radiation exposure (pre-rad) and after five years in orbit (post-rad). The spectral response curve of channel 4 therefore changes slowly and proportionally to the total radiation dose received. There is no in-orbit capability to directly verify the spectral passband. An empirical spot check validation of the spectral response curves using various ground test sites and algorithms in support of this validation are discussed in Section 3.3.
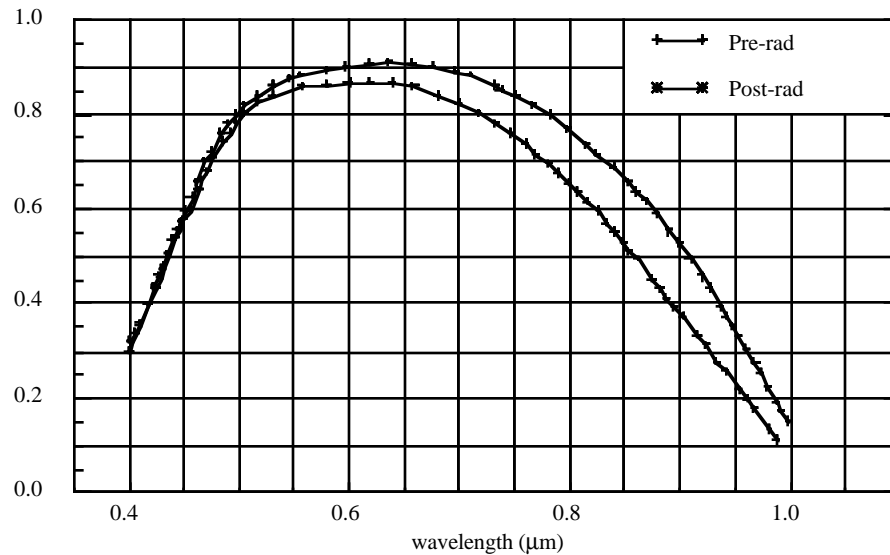
Figure 3.5

The relative response of the Si diode before radiation exposure (pre-rad) and after five years in orbit (post-rad).

3.1.1 Calibration Requirements

The sensor is designed to achieve better than 1% *relative* photometric accuracy at an albedo of unity. There is no absolute calibration accuracy requirement for the visible light sensors.

3.1.2 Calibration Devices

The onboard photometric calibration subsystem for the visible channels is shown in Fig. 3.6. It is comprised of three tungsten lamps (used one at a time - extra lamps provide redundancy), an imaging lens, a pair of Precision Reference Diodes (PRD) and a dark view.

3.1.2.1 Dark View.

The visible detectors view the infrared blackbody once every 2.667 seconds. The albedo of the blackbody in the visible, expected to be less than 0.01 (TBD), is part of the instrument characterization deliverables. The blackbody view provides the zero signal reference level.
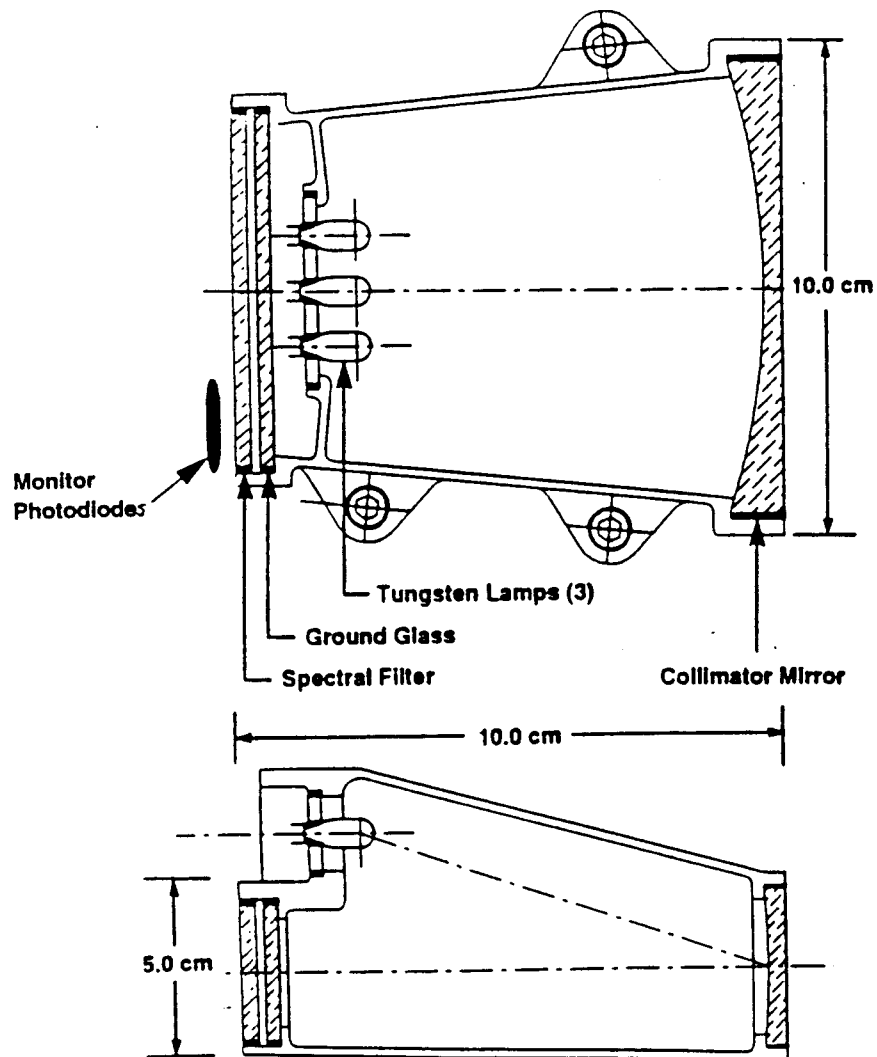
Figure 3.6

The onboard photometric calibration subsystem for the visible channels. It is comprised of tungsten lamps, an imaging lens, and a pair of Precision Reference Diodes.

3.1.2.2 Visible Light Calibration Source

The visible light calibration source uses three Welch Allyn No. 01178 lamps rated at 5.0 Volts, 0.44 amp. The filaments are operated at 4.5 Volts, 0.42 amp (1.9 Watts) to extend the lifetime. At 2.2 Watts input power, the filament has a lifetime of 1200 hours at a color temperature of 2925 K. The SNR for a single look at the calibration source is expected to be 15, 130, 320, and 177, in the four visible channels, respectively.

One of three tungsten lamps is operated for about 120 seconds once every second orbit (this is equivalent to 432 hours in 5 years). Since the filament output is expected to stabilize in about 10 seconds, measurements from 40 looks can be averaged to improve the effective SNR. A spectral filter is used to enhance the blue output of the filament. The output and color temperature of the lamp at a given input current changes as the filament ages. The output of the tungsten lamp/diffuser/lens assembly is therefore monitored by two PRD at two wavelength regions defined by the interference filter used for bands two and three. The effective filament color temperature and absolute radiance output can be obtained from the ratio and the summed output of the two PRD. The radiance output, R(obs), of this system as function of PRD output for a representative range of filament currents (i.e. filament temperatures) is calibrated pre-launch to about 20% absolute accuracy in all four channels and is part of the instrument characterization record. A temperature sensor monitors the temperature of the detectors to allow interpolation between calibration views.

The absolute calibration of the visible calibration system can be significantly improved relative to the prelaunch calibration through routine vicarious calibration using well characterized ground calibration sites. This process, error estimates and vicarious calibration update frequencies and relevant algorithms are described in Section 3.2.3.

3.1.3 Photometric Accuracy Estimate

The VIS/near IR sensor is required to achieve 1% relative photometric accuracy at an albedo of unity. Estimates made at the preliminary design review indicate that the design will achieve this requirement over the full five year mission lifetime. The leading components to the photometric error budget are the stability of the electronics subsystem and the stability of the photometric calibrator.

Response non-linearity in the detectors and electronics will be measured pre-launch and will be removed using table lookup or low-power polynomial fitting of the test data. Linearity changes occurring during the mission as a result of natural radiation exposure are expected to be less than 0.5%. The gain/offset stability is estimated to be 0.3%. The photometric calibrator contribution to the uncertainty is due to photo reference diode response stability (0.3%) and interlamp geometry differences (0.3%).

Signal-to-noise is not a contributor to photometric error. The predicted signal-to-noise ratio at an Earth albedo of 0.4 is 540 at the start of the mission, degrading to about 420 at the end of the five year mission, at a nominal sensor temperature of 30 C. If the residual non-linearity can be decreased using observations of ground targets with various radiances covering the dynamic range, then photometric accuracy of 0.5% may be achievable.

3.2 Calibration of AIRS VIS/NIR channels

3.2.1 Introduction

During the launch and operation phases of the EOS spacecraft the performance of the AIRS VIS and NIR channels are expected to change. This may be caused by a change of the sensor optics during launch or a change of sensitivity due to surface contamination or a change in the spectral response of the Si detectors arrays with the total dose of radiation received. The gain and offset of the electronics may also change with time while the instrument is in orbit. Though the photometric calibration assembly provides on-board calibration capabilities (Sec. 3.1) during operation, the calibration accuracy will decrease over time due to lamp degradation and changes within the optical system. Therefore, indirect calibration (vicarious calibration) with known ground surfaces and cross-calibration with other related instruments is necessary.

The radiometric calibration algorithm for AIRS VIS/NIR channels will correct for systematic effects caused by optical system degradation during launch and operation, change of offset and sensitivity of the detectors and electronics, change of spectral response of the detectors with total radiation dose and non-linearity of the A/D converters. Prelaunch calibration will provide the functional relationship between the digital counts and radiance. A look-up table will be used to correct the non-linearity to obtain the linearized calibration equation

$$R = \alpha * DN + \beta, \qquad \text{Eq. 3-1}$$

which can be rewritten as:

$$R = \alpha * (DN - DN_o) \qquad \text{Eq. 3-2}$$

where DN is the (linearized) digital output of the electronics in response to a radiance R received by a VIS/NIR channel, α and β are the gain and offset of the channel, respectively, and DN_o is the digital number corresponding to the dark view. Because a similar calibration algorithm applies to all four VIS/NIR channels, the channel number is not included in the calibration expressions.

Different level 2 data products have different calibration accuracy requirements. The accuracy of the radiance measurement can be refined in three steps, with increasing absolute accuracy and algorithmic and operational complexity.

Step I: Makes use of the onboard calibration source to correct the gain.

Step II: Makes use of the onboard calibration source to correct the gain and uses ground based sites (vicarious calibration) to determine a gain correction term.

Step III: Makes use of the onboard calibration source to correct the gain, then uses data from other instruments on the same spacecraft to deduce a gain correction term, γ.

$$R = \gamma \, \alpha \, (DN - DN_o). \qquad \text{Eq. 3-3}$$

The routine calibration algorithm is based entirely on Step I, with the multiplicative gain correction term set equal to unity. Step II will we done off-line at a team member facility on a monthly (TBD) basis, resulting in the delivery of a table of multiplicative correction coefficients to the onboard calibration. Step III is a research product to be developed at a team member facility. Although the concept of this algorithm will be discussed, details of the algorithm are outside of the scope of this ATBD.

3.2.2 On-Board Calibration

For Step I the on-board photometric calibration equipment described in Section 3.1 will be used to calibrate changes in offset and gain.

3.2.2.1 Calibration of the gain

The visible detectors view the infrared blackbody every 2.667 seconds. The zero signal reference level of the dark view will be used for calibration of the change in offset.

The dark view and tungsten lamps are used to determine DN_o and α on-board. We have:

$$\alpha(ob) = \frac{R(ob)}{DN(ob) - DN_o(ob)} \qquad \text{Eq. 3-4}$$

where $DN_o(ob)$ is the digital number of dark view, $R(ob)$ is the equivalent radiance of the tungsten lamp for on-board calibration (Section 3.1). The label "ob" is used to denote On-Board calibration.

The non-linearity of the photodiodes and their associated electronics will be corrected for by setting up lookup tables of alpha as a function of DN. The four detector arrays, each with 9 elements, will result in 36 tables. The lookup tables will initially be set using data from the prelaunch characterization of the instrument.

3.2.3 Vicarious Calibration

An improvement in the calibration accuracy is achieved in Step II. There are many vicarious calibration techniques which all have strengths and weaknesses. They include ground-based, aircraft based, satellite-based, buoy based and lunar observations (Abel, 1991; Brest and Rossow, 1992; Che et al. 1991; Che and Price, 1992; Fraser and Kaufman 1985; Holben et

al. 1990; Price, 1987; Slater et al. 1987). Note that "ground-based" is used here to mean based upon observations of the ground from orbit. The goal of these techniques is to estimate the radiance at the instrument aperture given an observation from one or more instruments and/or a calculation from a radiative transfer model. These techniques are used to obtain the gain of the instrument but cannot provide, in general, the offset. The absolute calibration of the AIRS VIS/NIR system can be significantly improved relative to the 20% prelaunch calibration through ground-based calibration of the gain.

3.2.3.1 Theoretical Basis

A ground-based vicarious calibration must be done with known, homogeneous ground surface targets with relatively high surface reflectance. The area should be large enough to ensure complete coverage by one sensor pixel. Clear sky over a sand surface, such as White Sands in New Mexico, or other desert areas are good targets (Frouin and Gautier, 1987; Slater et al., 1991 and Guenther, et al., 1990). In order to produce reliable ground-based calibrations, an accurate estimation of the surface reflectivity, the aerosol type and concentration, and the atmospheric profile, particularly the water vapor column density, is essential. (Spectral reflectivity of a sand surface is related to its moisture content. The difference between dry and wet sand reflectivities in the Visible and NIR wavelengths can be as much as 15% [Walraven and Coulson, 1972].) If the solar and viewing zenith angles and relative azimuth angle of the ground objects are large, the BRDF effects must be taken into account. Thus, an accurate measurement (or model) of the target's spectral bi-directional reflectivity is necessary. It has been estimated that the absolute radiometric calibration accuracy that can be obtained using this ground-based approach is better than 13% (Frouin and Gautier, 1987).

3.2.3.2 Sensitivity Analysis

To evaluate the sensitivity of the calibration to the effects discussed above we have used a radiative transfer model (SBDART, Ricchiazzi et al., 1996). Figure 3.7 displays the calculated flux for AIRS channels 1 through 4 over a sand surface and cloudless sky as a function of aerosol visibility, atmospheric profile, and aerosol types. It can be seen that aerosol type and visibility has a significant effect on channels 1 and 2, specifically when the visibility is low; while the water vapor amount has a significant effect on channels 3 and 4.
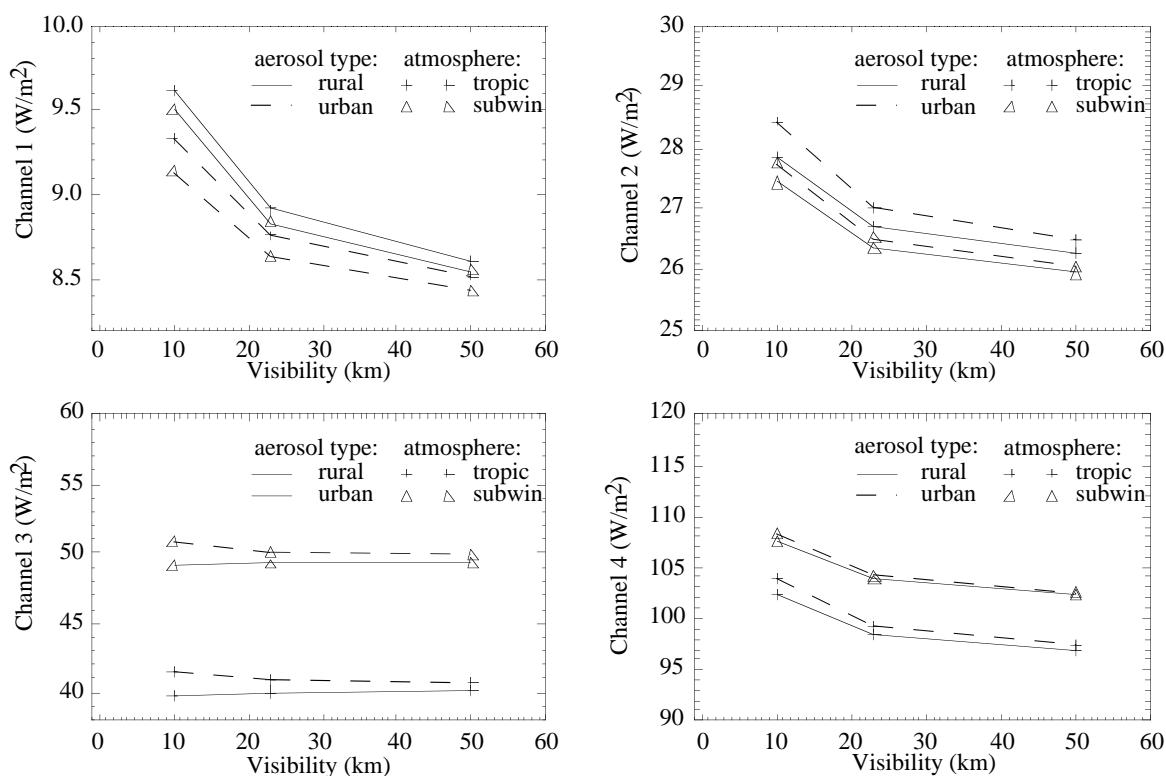
Figure 3.7

The calculated flux for AIRS channels 1 through 4 over a sand surface and cloudless sky as a function of aerosol visibility at different atmospheric profiles and aerosol types at a 30 degree solar zenith angle.

3.2.3.3 Data Destripping

The ground calibration target area should be homogeneous and large (e.g., White Sands, New Mexico). Though the non-linearity of detectors and electronics will have been corrected prior to launch, strips due to the array of detectors may still be present in the VIS/NIR data over homogeneous regions. A destripping procedure taking an average of 9 pixels along track would require too large an homogeneous target area. Instead, a moving window method, taking an average of 3 pixels along track, will be applied.

3.2.3.4 Application

Suppose the radiance calculated by the RT model is R(g) and the measured digital number is DN(g), where the subscript g is used to denote ground-based calibration, then:

$$\alpha(g) = \frac{R(g)}{DN(g) - DN_o(g)} \qquad \text{Eq. 3-5}$$

The correction coefficient from ground-based calibration for α is then:

$$\gamma(g) = \frac{\alpha(g)}{\alpha(ob)} \qquad \text{Eq. 3-6}$$

(No information about DN_o can be obtained from the ground-based calibration and none is needed, since the blackbody view on every scan line is a very good zero radiance for the visible channels.)

The ground-based calibration will require clear sky atmospheric conditions. Atmospheric temperature and moisture profiles will be obtained from AIRS IR and AMSU products. Aerosol conditions will be determined from the visibility reported by the closest meteorological station or airport (e.g. HMN, a station a few km from the White Sands target area). Rural or continental aerosol types will be used. The surface type at White Sands is well characterized, except when wet. Precipitation events over White Sands will be monitored to determine appropriate times for calibration measurements. Surface BRDF will be either measured or modeled. A 3-D surface model is being developed for that purpose. The ground-based calibration will be carried out on a monthly basis during the operational phase.

3.2.4 Cross-Calibration with MODIS

3.2.4.1 Theoretical Basis

Step III for improving the absolute calibration is to use cross-calibration of the AIRS VIS/NIR with other instruments on the same platform, in this case with MODIS. In the MODIS Spectral and Radiometric Calibration Assembly (SRCA), the NIST standard is transferred to the SRCA. The SRCA will transfer the calibration to the Solar Diffuser and Solar Diffuser Stability Monitor (SD/SDSM) during the activation and evaluation phase of the instrument. The absolute radiometric uncertainty is expected to be smaller than 4.6% in-orbit (Jones, et al., 1995). The AIRS VIS/NIR channels cross-calibration uses a linear combination of MODIS channels. The following is the concept description. The approach will be fully developed as a research product.

Let $AIRS_i$ be the radiance from a pixel of AIRS channel i and $MODIS_j$ is the radiance from an AIRS spatially equivalent MODIS measurement from channel j. Since the AIRS FOV full width at half peak, 2250 meters at nadir, is much larger than MODIS pixels at the wavelengths in question, typically 250 to 1000 meters at nadir, AIRS spatially equivalent pixels are, in principle, obtained by convolving a gridded image of a calibration site using MODIS channel j with the AIRS spatial response function. Since the cross-calibration sites

will typically be relatively homogeneous (and cloud free) desert surfaces, the requirement for registration accuracy between the MODIS and AIRS pixels for calibration purpose is relatively loose and the pre-launch determined AIRS pixel spatial response functions will be adequate.

Figure 3.8 shows the AIRS VIS/NIR channels 1 through 4 overlaid with the spectrally similar MODIS channels. Transmittance and spectral surface albedo are plotted on the same figure. The coverage of the AIRS and MODIS channels displayed in Figure 3.8 are listed in Table 3.1.

Many MODIS channels overlap, but only the non-overlapping and evenly distributed MODIS channels will be linearly combined to cross-calibrate the AIRS channels. Hence, $AIRS_1$ will be cross-calibrated with $MODIS_8$ and $MODIS_9$. $AIRS_2$ will be cross-calibrated with $MODIS_1$ and $MODIS_{14}$. Because $AIRS_2$ includes water vapor absorption bands but $MODIS_1$ and $MODIS_{14}$ exclude water vapor absorption bands, $MODIS_{19}$ will be added to account for water vapor absorption. $AIRS_3$ will be cross-calibrated with $MODIS_2$, $MODIS_{15}$ and $MODIS_{19}$, and $AIRS_4$ with $MODIS_1$, $MODIS_2$, $MODIS_3$, $MODIS_4$, $MODIS_8$, $MODIS_{15}$, $MODIS_{19}$. This cross-calibration will be done using multivariable regressions as follows:

$$AIRS_1 = a_0 + a_1 \cdot MODIS_8 + a_2 \cdot MODIS_9 \qquad \text{Eq. 3-7}$$

$$AIRS_2 = a_0 + a_1 \cdot MODIS_1 + a_2 \cdot MODIS_{14} + a_3 \cdot MODIS_{19} \qquad \text{Eq. 3-8}$$

$$AIRS_3 = a_0 + a_1 \cdot MODIS_2 + a_2 \cdot MODIS_{15} + a_3 \cdot MODIS_{19} \qquad \text{Eq. 3-9}$$

$$AIRS_4 = a_0 + a_1 \cdot MODIS_1 + a_2 \cdot MODIS_2$$
$$+ a_3 \cdot MODIS_3 + a_4 \cdot MODIS_4$$
$$+ a_5 \cdot MODIS_8 + a_6 \cdot MODIS_{15} + a_7 \cdot MODIS_{19} \qquad \text{Eq. 3-10}$$

where, for brevity, we use the same coefficient symbols in each of the above equations, but it is understood that a_x in one equation is independent of a_x in any other equation.

The coefficients a_0, a_1, ..., will be obtained using multivariate linear regression of the measured AIRS and MODIS digital numbers or radiance data.
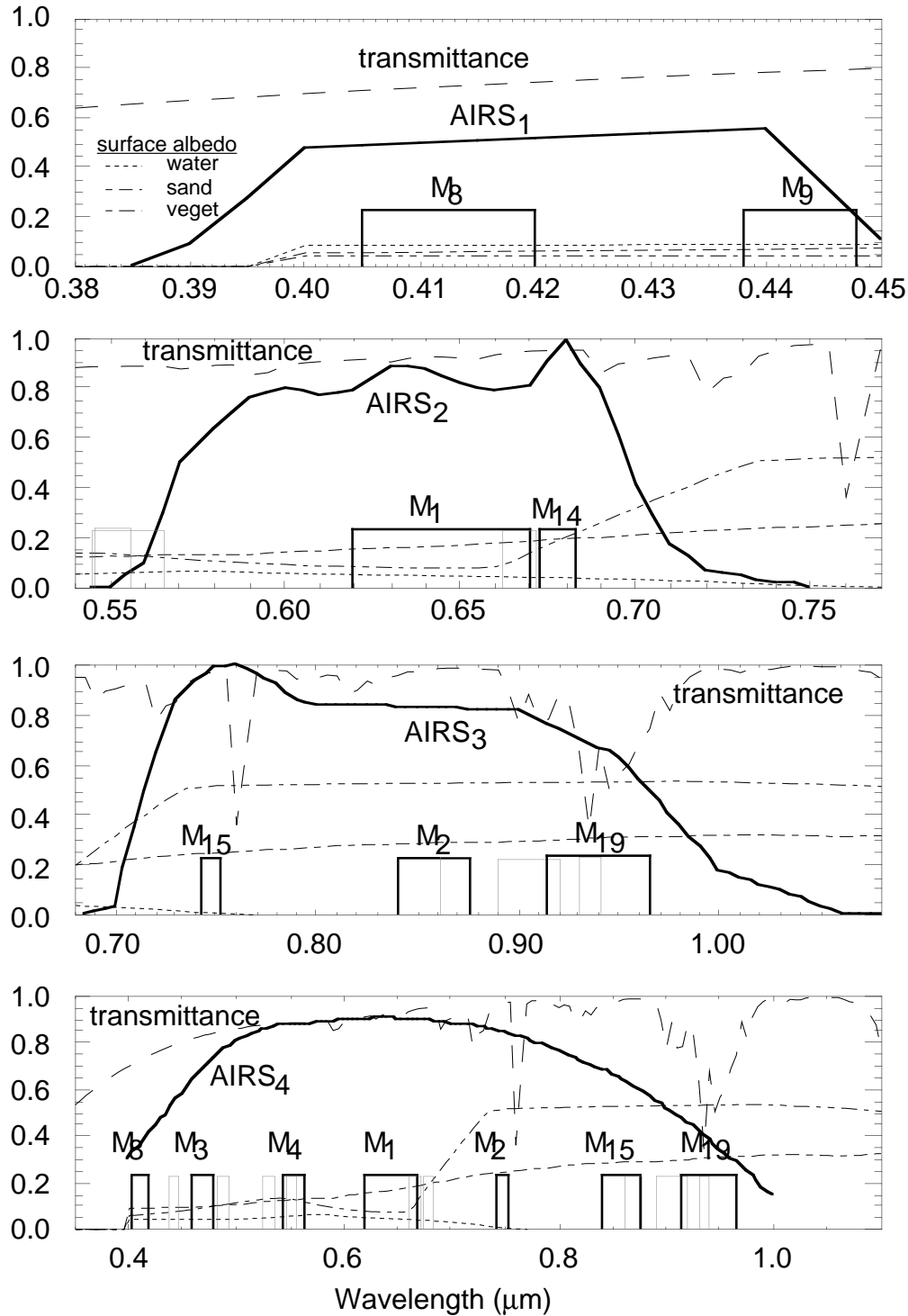
Figure 3.8

AIRS VIS/NIR channels 1 through 4 overlaid with the spectrally similar MODIS channels. Transmittance and spectral surface albedo are plotted on the same figure.

It is necessary to determine what specific surface and atmospheric conditions will be most suitable for the AIRS and MODIS cross-calibration. We know that data acquired from desert area in clear sky are the best data for cross-calibration. However, we need to determine how the atmospheric profiles, specifically water vapor content, change of aerosol types and concentration, thin clouds (which may not be seen by AIRS VIS/NIR channels) and randomly distributed shrubs and shadows in the target region will affect the cross-calibration results. For this purpose, we calculated AIRS and related MODIS radiances using the SBDART radiative transfer model under the following conditions:

a) Surface cover: sand and vegetation.

b) Atmospheric profile: TROPIC, SUBWIN (subarctic winter) and US62 (standard US atmosphere), with water vapor column densities 4.12, 0.85 and 4.2 g/cm^2 respectively.

c) Cloud optical thickness: 0, 1 and 2.

d) Cloud layers: 0-1, 1-2, 2-3 and 3-4 km.

e) Cloud droplet size effective radius: 4, 8, 16 and 106 μm (cloud top height at 10 km for 106 μm cirrus cloud).

f) Aerosol type: rural, oceanic and urban.

g) Visibility: 10, 23 and 50 km.

The coefficients, a_i, of the linear equations (3-7) through (3-10) are calculated with three types of conditions (i) sand surface in clear sky, (ii) sand surface in clear sky and slightly cloudy (meaning optical depth less than 3) and, (iii) sand and vegetation surfaces in clear sky and slightly cloudy conditions. All combinations of atmospheric conditions (atmospheric profiles, aerosols and visibilities) were included in these calculations.

The linear combination of MODIS channels with respect to AIRS channels, and their fitted lines are plotted in Figure 3.9 and Figure 3.10 (W/m^2 is used in the plots). The coefficients of the linear equations a_i, the correlation coefficients and standard deviation are listed in Table 3.2.
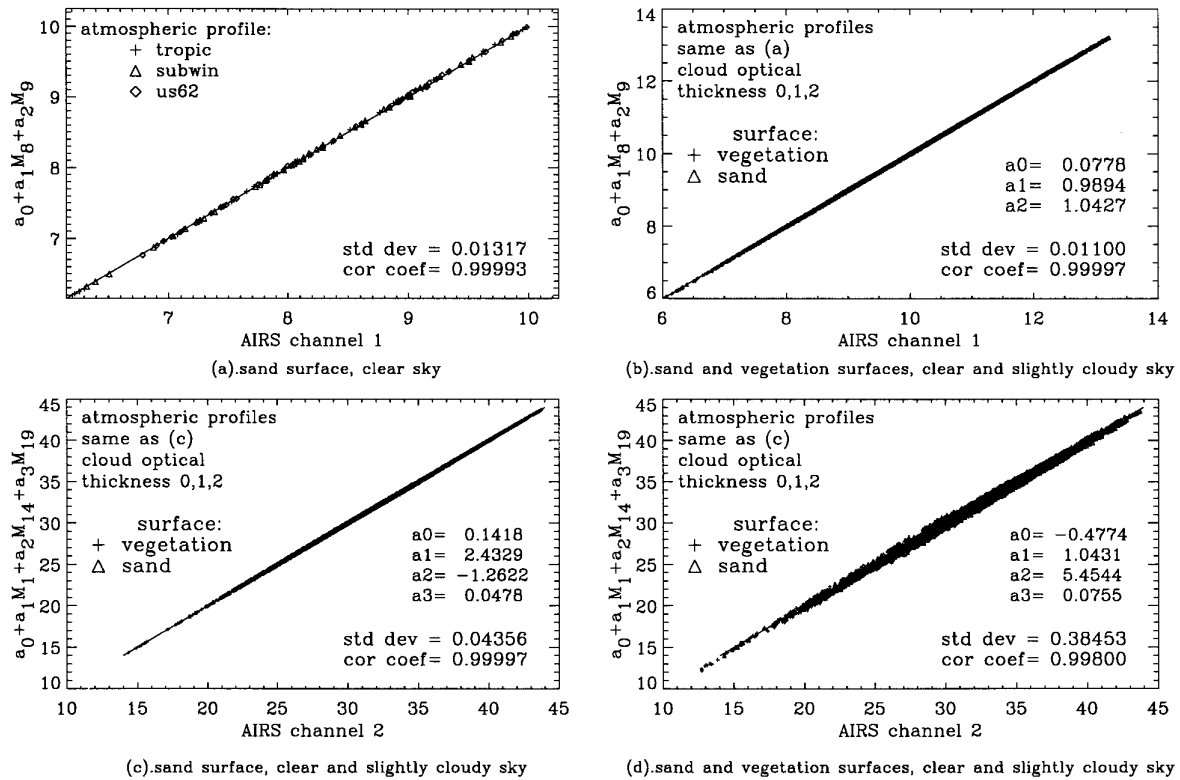
Figure 3.9

Cross-calibration of AIRS channel 1 (a and b) and 2 (c and d) using MODIS data. Panels (a) and (c) show the accuracy with which the cross-calibration can be achieved for sand surfaces. Panel (b) indicates that, even with a vegetated surface, the Ch. 1 cross-calibration is successful. For Ch. 2, however, the calibration is much poorer if vegetation is present (panel d). In these plots, calculations were made for 3 atmospheric profiles, 5 solar zenith angles, 3 aerosol types with 3 visibilities each, cloud optical thickness 0, 1 and 2 with 4 effective radii and 5 heights.

It can be seen that for *AIRS*1 and *AIRS*4, the coefficients calculated from sand and vegetated surfaces, in clear sky and slightly cloudy conditions, (Fig. 3.9.b and Fig. 3.10.d) can be applied to the data calculated from sand surfaces in clear sky, as well (Fig. 3.9.a and 3.10.c). On the other hand, for channels 2 and 3, the correlation in the presence of vegetation (Fig. 3.9.d and 3.10.b) is much poorer than in the pure sand case (Fig. 3.9.c and 3.10.a).
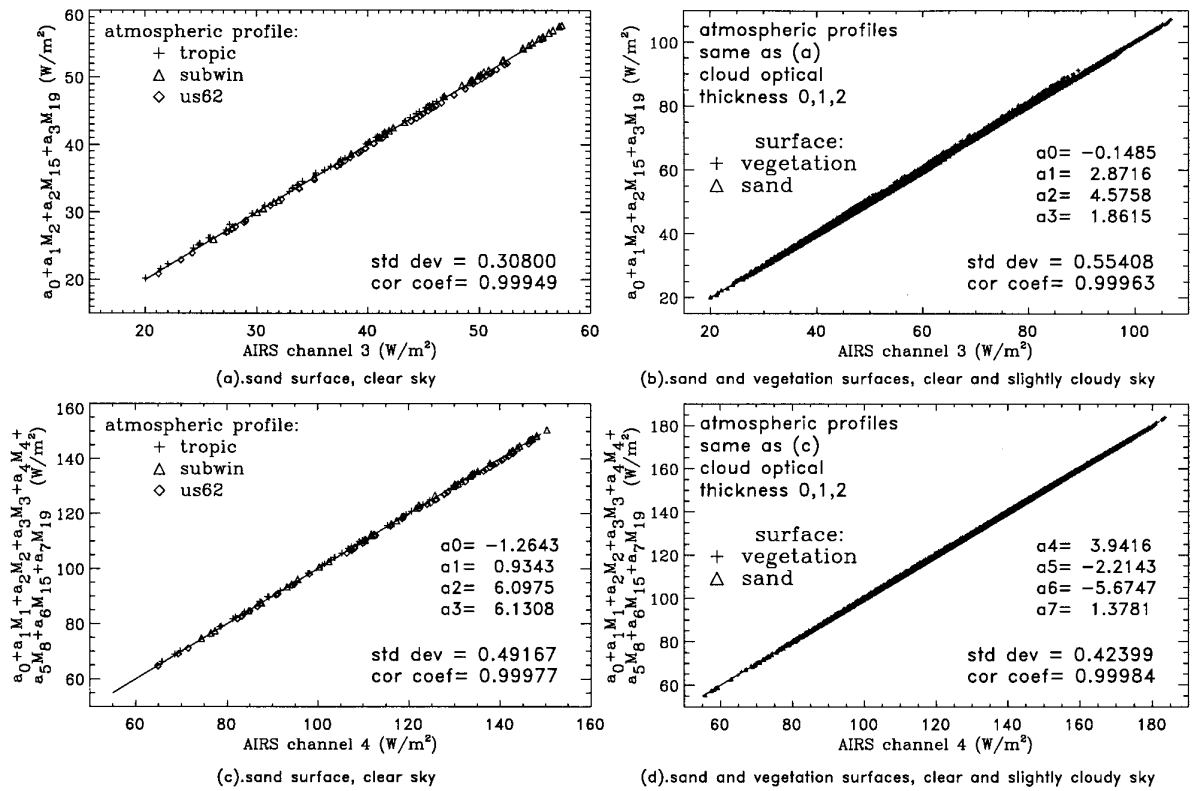
Figure 3.10

Cross-calibration of AIRS channel 3 (a and b) and 4 (c and d) using MODIS data. As in Fig. 3.9, calculations were made with 3 Atmospheric profiles, 5 solar zenith angles, 3 aerosol types with 3 visibilities each, cloud optical thickness 0, 1 and 2 with 4 effective radii at 5 heights.

This implies that only a pure desert area like White Sands, New Mexico can be used as a ground target for $AIRS_2$ and $AIRS_3$ cross-calibration. However, desert and semi-desert areas can be used as ground targets for $AIRS_1$ and $AIRS_4$ cross-calibration. The acceptable ground targets for the cross-calibration of $AIRS_1$ and $AIRS_4$ are therefore more abundant. It can also be seen that only the surface albedo has a significant effect on the accuracy of the cross-calibration. The influence of the atmospheric profile, aerosol type, visibility, and layer of thin clouds on the cross-calibration is negligible. This means that, unlike the ground-based calibration, no local meteorological or surface condition data are required for the cross-calibration. Therefore, the cross-calibration can be performed as frequently as required.

AIRS channel	wave range (µm)	MODIS channel	wave range (µm)
1	**0.400-0.440**	**8**	**0.405-0.420**
		9	**0.438-0.448**
2	**0.550-0.745**	**1**	**0.620-0.670**
		14	**0.673-0.683**
3	**0.690-1.100**	**15**	**0.743-0.753**
		2	**0.841-0.876**
		19	**0.915-0.965**
4	**0.400-1.000**	**8**	**0.405-0.420**
		3	**0.459-0.479**
		4	**0.545-0.565**
		1	**0.620-0.670**
		15	**0.743-0.753**
		19	**0.915-0.965**

Table 3.1. AIRS and related MODIS channels

Figure 3.11.a and Figure 3.11.b show the $AIRS_4$ radiance as a function of the linear combination of MODIS radiance data, similar to Fig 3.10, but for expected beginning and end of life conditions. The $AIRS_4$ radiance can be fit with a line:

$$AIRS_4 = b_0 + b_1 \cdot x \qquad \qquad \text{Eq. 3-11}$$

where:

$$x = a_0 + a_1 MODIS_1 + a_2 MODIS_2 + a_3 MODIS_3$$
$$+ a_4 MODIS_4 + a_5 MODIS_8 + a_6 MODIS_{15}$$
$$+ a_7 MODIS_{19} \qquad \text{Eq. 3-12}$$

The coefficients a_i are listed in last column of Table 3.2.

(a).sand surface, clear sky   (b).sand and vegetation surfaces, clear and slightly cloudy sky
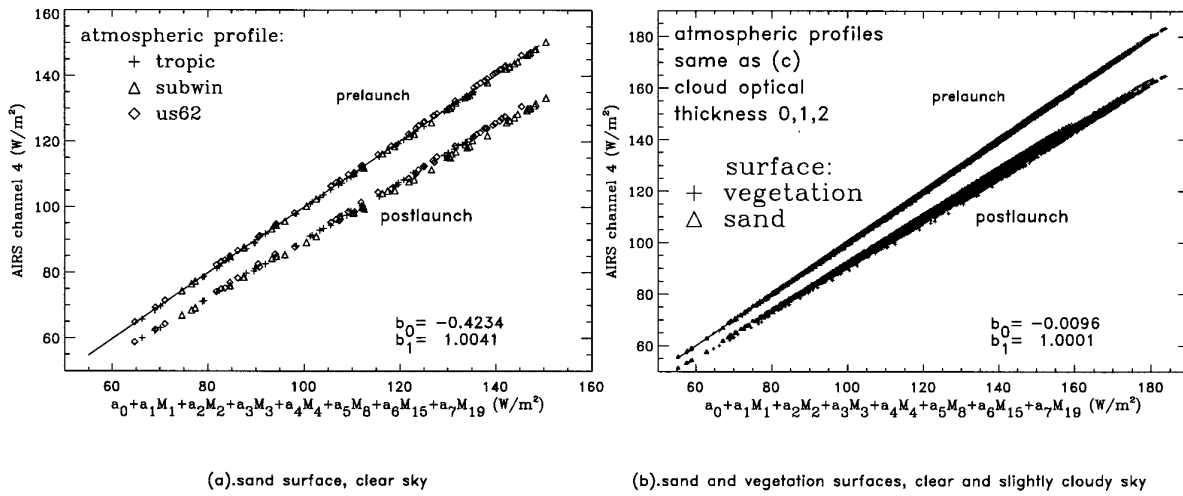
Figure 3.11

Cross-calibration of AIRS channel 4 using MODIS data same as Figure 3.10 (c) and (d). The coefficients are calculated using prelaunch spectral response (upper) and the estimated spectral response of channel 4 after 5 years in-orbit (postlaunch, lower).

After 5 years in orbit, the spectral response of $AIRS4$ is expected to degrade as shown in Figure 3.5. $AIRS4$ will have less output signal over the same ground targets as shown by the lower fitted lines of Figure 3.11a and Figure 3.11b. $AIRS4$ data can be restored to beginning of life equivalent values using Eq. 3-11 and Eq. 3-12.

The coefficients a_i in Table 3.2 are calculated based on a radiative transfer model. For practical applications, they should be calculated using real AIRS VIS/NIR and corresponding MODIS radiance data over the same ground targets to perform this cross-calibration. Therefore, it is important to spatially register the AIRS VIS/NIR channels with MODIS channels. Since a homogeneous desert surface is the best calibration area, the requirements for registration accuracy between the two is very loose for calibration purposes.

(a). AIRS channel 4 with respect to MODIS channel 15

(b). AIRS channel 4 with respect to MODIS channel 3
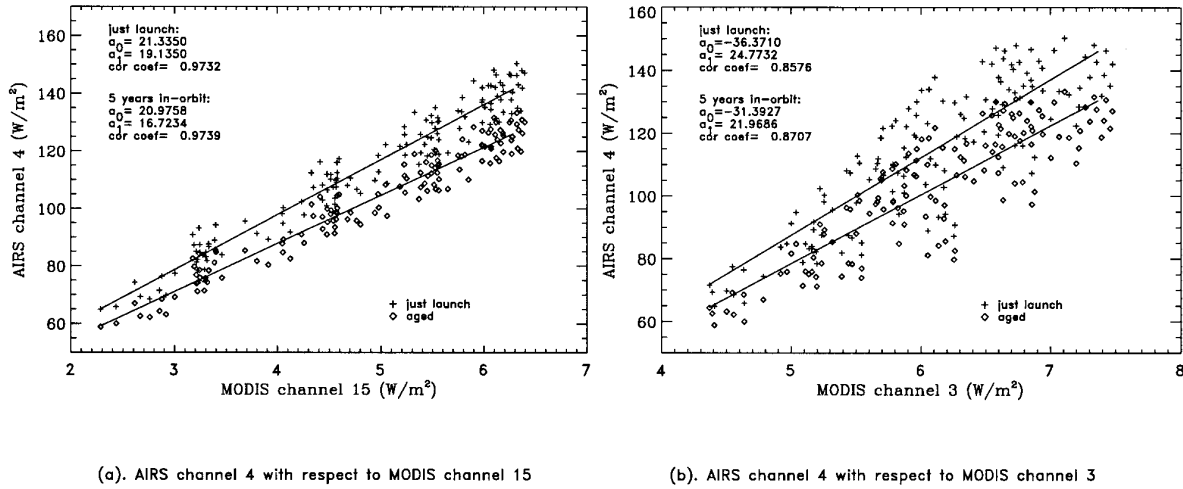
Figure 3.12

The change of spectral response of AIRS channel 4 can be detected by the ratio of AIRS channel 4 to MODIS channel 15 (left) over a vegetated surface in clear sky conditions. The atmospheric profile and aerosols have a stronger effect on MODIS Channel 3.

	channel 1	channel 2	channel 3	channel 4
a_0	0.0778	0.1418	-0.1485	-1.2643
a_1	0.9894	2.4329	2.8716	0.9343
a_2	1.0427	-1.2622	4.5758	6.0975
a_3			1.8615	6.1308
a_4				3.9416
a_5				-2.2143
a_6				1.3781
Maximum difference (%)	0.366 [b]	0.577 [a]	2.26 [a]	1.18 [b]
standard deviation	0.011 [b]	0.0223 [a]	0.308 [a]	0.424 [b]

Table 3.2. Calculated coefficients of linear combinations of MODIS channels in Eq. 3-7 through Eq. 3-10: maximum difference between AIRS data and the fitted lines (in percentage): and the standard deviation. a. - sand surface as ground target b.- sand and vegetation as ground target.

3.2.4.2 Application

The cross-calibration establishes the relationship between the digital number and the radiance for AIRS VIS/NIR channels. After launch, in the evaluation phase, the relationship between

digital number of AIRS VIS/NIR channels and the linear combination of corresponding digital numbers of MODIS channel over the target areas given by:

$$DN(e) - DN_o(ob) = a_0 + a_1 * DNM(i_1) + a_2 * DNM(i_2) + ... \qquad \text{Eq. 3-13}$$

will be established as soon as possible, DN(e) and DNM are the AIRS and corresponding MODIS digital numbers in the target areas during the cross-calibration evaluation phase. The coefficients a_0, a_1, a_2 etc. will be used later on for cross-calibration.

In the operational phase, AIRS measured digital numbers, DN, will be used to calculate the coefficient $\gamma(M)$:

$$\gamma(M) = \frac{DN(e) - DN_o(ob)}{DN(ob) - DN_o(ob)}. \qquad \text{Eq. 3-14}$$

$\gamma(M)$ will be used to correct the degradation of the AIRS VIS/NIR channels. Similar to the ground-based calibration, no information about DN_o is provided by or necessary for the cross-calibration.

Only general ground target and atmospheric condition information will be required for cross-calibration, so it will be carried out on a daily basis during the evaluation phase and on a weekly basis during the operational phase.

3.2.4.3 Calibration Expression

The calibration expression, Eq. 3-2, becomes

$$R = \alpha*(DN - DN_o) = \alpha(ob) * \gamma(g) * \gamma(M) * [DN - DN_o(ob)]. \qquad \text{Eq. 3-15}$$

The correction coefficients $\alpha(ob)$, $\gamma(g)$ and $\gamma(M)$ may change with time. A plot of these coefficients with respect to time will be used to study the degree and trend of the instrument degradation.

3.3 Spectral Calibration of AIRS VIS/NIR Channels

The spectral response of $AIRS_1$ through $AIRS_3$ visible channels is controlled by an interference filter and the spectral characteristics of an Si photodiode. The *AIRS4* channel is controlled by the spectral characteristics of the Si photodiode only. There is no on-board spectral calibration capability in the AIRS VIS/NIR instrument. However, the spectral response of the Si detectors usually shifts slowly to shorter wavelength as a function of total radiation dose. The spectral response of the interference filter may change with time as well.

Detection of change in AIRS VIS/NIR spectral response may be required. Because of the low spatial resolution of AIRS VIS/NIR channels (2.2 km), there is no homogeneous ground object which has spectral reflectivity sharp enough for spectral calibration. The ground-based and cross-calibration with MODIS channels used in radiometric calibration cannot provide accurate enough spectral calibration even though the accuracy of MODIS spectral response can be calibrated to ± 1 *nm* for waveband less than 1.0 *μm.*

The degradation of the spectral response of the Si photodiode will only be roughly estimated. Two approaches will be used. For $AIRS_2$ and $AIRS_3$, we will use the Amazon forest as a ground reference and the vegetation index as the parameter to monitor. The Vegetation Index is defined as:

$$VI = \frac{AIRS_3 - AIRS_2}{AIRS_3 + AIRS_2}. \qquad \text{Eq. 3-16}$$

We will monitor the maximum value of the Vegetation Index of the Amazon forest measured by $AIRS_2$ and $AIRS_3$ to detect changes in the spectral characteristics of the system.

For evaluating the change of $AIRS_4$ spectral response, $MODIS_{15}$ (0.743-0.753) radiance can be used over any vegetation surfaces in clear sky conditions. Using the prelaunch spectral response of $AIRS_4$, the relationship between $AIRS_4$ and $MODIS_{15}$ is

$$AIRS_4 = 21.335 + 19.135 \; MODIS_{15}. \qquad \text{Eq. 3-17}$$

Due to the change of $AIRS_4$ spectral response after 5 years in operation, it is expected to change to:

$$AIRS_4 = 20.976 + 16.723 \; MODIS_{15}. \qquad \text{Eq. 3-18}$$

The correlation coefficient between these two channels is as high as 0.974. $MODIS_{15}$ is in the atmospheric window and in the longwave side of the $AIRS_4$ channel, hence it is least affected by water vapor content and aerosol type and concentration (Figure 3.12a). As a comparison, the correlation coefficient of $AIRS_4$ to other MODIS channels is much smaller as shown by the plot of $AIRS_4$ with respect to $MODIS_3$ (Figure 3.12b).

3.4 Spatial Calibration

This section describes how the four visible/near-infrared channels will be spatially calibrated with respect to each other, with respect to absolute coordinates on the Earth's surface, and with respect to the infrared footprint. The creation of maps and common grids for visible and infrared data are briefly discussed, along with some considerations for co-alignment of the AIRS and MODIS instruments.

For this discussion, it is useful to refer again to Fig. 3.2. As was described previously, the term "visible pixel" is used to describe a square region on a detector, 250 μm by 250 μm. Each pixel, however, is composed of 10 sub-elements, a sub-element being 250 μm in the scan direction, $\hat{y}$, but only 25 μm along the array axis, $\hat{x}$. *As originally envisioned, only one element of each pixel would be sampled, leaving 90% of a pixel's area unobserved. Consideration is currently being given to sampling all elements to provide complete coverage: in the discussion to follow, it is assumed that this is done. If the final design does not include sampling of all pixel sub-elements, straightforward revisions to the coastline location algorithm and error analysis presented here will be necessary.* Due to instrument scan motion and the finite readout time between sub-elements, each sub-element will be displaced in the y-direction relative to the previous one. We take this displacement to be 0.16% of the sub-element's long axis (the y-axis).

The instrument specifications call for the visible channels to have $\hat{x}$ and $\hat{y}$ offsets of ≤ 25 micron (10% of a visible pixel), to be aligned along the $\hat{x}$ direction to within 0.001 radians, and to be boresighted with the IR field-of-view to within 1 pixel. On-orbit spatial calibration will improve upon these values. It will be shown that the limiting factor in determining the spatial orientation is our *a priori* knowledge of the rotational state of each linear array and, as a practical limit, spatial orientation cannot be determined to better than 1% of a pixel (about 0.00185°). This accuracy is more than sufficient for all anticipated uses.

3.4.1 Relative Spatial Calibration of the Visible Channels

The first level of calibration is to determine the offsets of three of the detector arrays from the remaining one. This allows all visible data to be brought into a common coordinate system. Any of the channels may be used as the reference, but noise and surface sensitivity considerations discussed later suggest Channel 1 should be avoided. The output of this relative calibration will be three quantities for each channel: ΔX (the $\hat{x}$ displacement of one array relative to the reference array), ΔY (the $\hat{y}$ displacement of one array relative to the reference), and ϕ (the angle between the instrument's x-axis and the centerline of the array). (See Fig. 3.13.) For the reference array, ΔX and ΔY will be identically zero, though its ϕ may be non-zero. Note that it is currently assumed that one set of offsets can be used for every pixel within an array. If it is later determined that each pixel must be independently calibrated, the technique described here is still valid.

The location of a coastline as observed by two different channels can be used to determine the offsets between those channels. Therefore, consider how a coastline may be located within any channel (Fig. 3.13). Assume the ocean and land surfaces are homogenous, and that the coastline is straight. Under these conditions, the observed radiances from ocean, land, and mixed pixels will be distinct and recognizable. If R_O is the radiance from an ocean pixel, R_L

the radiance from a land pixel, and R_{Mix} the radiance from the pixel containing the coastline, the point where the coast intersects the center-line of the array within the "mixed" pixel, d′, is

$$d' = \left(\frac{R_{Mix} - R_O}{R_L - R_O} \right)$$

Eq. 3-19

where d′ is measured in units of a pixel-side. It is important to note that d′ is measured along the instantaneous array axis, and hence can be determined from the data without any geometric corrections. This expression is only valid for the simple geometry shown, where the coastline intersects both sides of the mixed ocean/land pixel, and there is only one mixed pixel. If the shoreline intersects more than one pixel, there are three possible forms for d′. If the shoreline intersects the side and bottom of a pixel,

$$d' = \frac{1}{\tan(\theta)} \left(0.5 - \sqrt{2\tan(\theta) \frac{R_{Mix} - R_O}{R_O - R_L}} \right).$$

Eq. 3-20

If the shore intersects the top and side of a pixel,

$$d' = 1 - \frac{1}{\tan(\theta)} \left(0.5 - \sqrt{2\tan(\theta) \frac{R_{Mix} - R_O}{R_O - R_L}} \right),$$

Eq. 3-21

and if the shore intersects both the top and bottom of a pixel,

$$d' = \frac{1}{2} \left[1 + \frac{1}{\tan(\theta)} \right] - \frac{R_{Mix} - R_O}{R_L - R_O} \frac{1}{\tan(\theta)}.$$

Eq. 3-22

One can determine which geometry applies by inspection of the observed radiances, and their transition between ocean and land values. The shoreline angle, θ, is known either from knowledge of the spacecraft ephemeris, or it can be determined from mapping of the visible data, which is described later. For optimum performance, the atmosphere should be clear and homogenous, the ocean and land surfaces should also be homogenous, and the coastline should be straight.
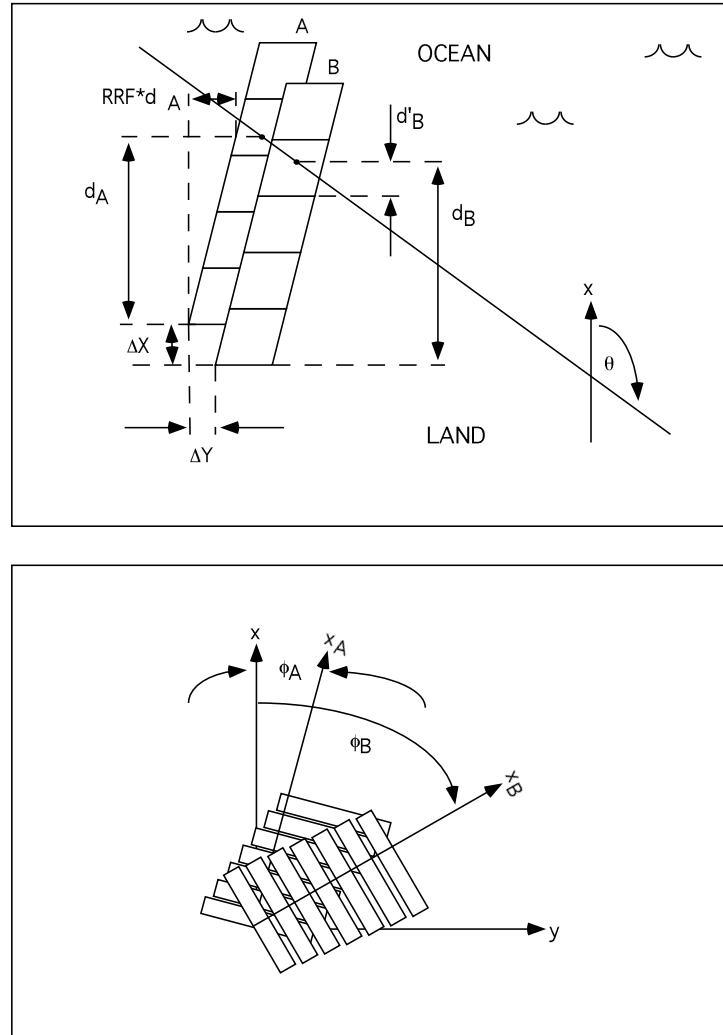
Figure 3.13

Near-nadir projections of visible pixels on the ground, and the coastline crossing geometry. The top diagram shows the relative offsets between pixels of the reference channel, A, and a channel B. As shown, φ is zero for both arrays. The instrument x-axis is shown, making an angle θ with the coastline. Due to scanning in the y direction, the projection of each array is offset an amount RRF per unit distance in the x-direction. For AIRS, RRF = 0.016. The coastline location, d, is always measured along the instantaneous long-axis of an array.

The bottom panel shows the effects of the arrays being rotated from the x-axis. x_A and x_B are the long axes of arrays A and B. As each pixel element is read in turn, there is an offset in the y direction due to scan motion. This creates tiny gaps (or overlaps for φ < 0) in the ground projection of the pixel sub-elements. If φ is 0.001 radians, however, the area of gaps is less than 0.02% of the area sampled.

If we assume the uncertainty in determining d′ is only due to errors in the measured radiances (which means a suitably homogeneous and straight coastline is being observed), then the uncertainty in locating the coastline, in units of pixel length, is

$$U_d = n \sqrt{\left(\frac{\partial d'}{\partial R_L}\right)^2 + \left(\frac{\partial d'}{\partial R_O}\right)^2 + \left(\frac{\partial d'}{\partial R_{Mix}}\right)^2} , \qquad \text{Eq. 3-23}$$

where n is the noise level of each measurement. (Atmospheric scattering and the VIS/NIR optics may also blur the distinction between ocean and land. The need for image restoration and deblurring techniques will be considered in the future.)

Doing this calculation, it can be shown that the maximum uncertainty expected for the first coastline geometry described above is

$$U_d = \frac{n\sqrt{2}}{R_L - R_O} . \qquad \text{Eq. 3-24}$$

For the last geometry described above (coastline intersects the top and bottom of a pixel), U_d is the same as Eq. 3-24, except for a factor of $1/\tan(\theta)$ on the right hand side. Taking θ to be near 45 degrees, however, this reduces to the same expression as Eq. 3-24.

For the intermediate geometries, the form of U_d is more complicated. Assuming reasonable values for θ and R_{Mix} (such as $\theta = 45°$ and $R_{Mix} = (R_L + R_O)/2$) yields values comparable to that shown above. Equation 3-24 will therefore be used in what follows as an estimate of the uncertainty in determining the coastline location within the array of any one channel.

From consideration of Fig. 3.13, the difference in coastline location between two channels is found to be related to the four offsets ΔX, ΔY, ϕ_A, and ϕ_B by

$$d_A - d_B = \Delta X \left(1 - \frac{RRF}{\tan(\theta)}\right) - \frac{\Delta Y}{\tan(\theta)} +$$

$$+ \frac{1}{RRF - \tan(\theta)} \left(\phi_B \left(\frac{\tan(\theta)}{2} + d_B\right) - \phi_A \left(\frac{\tan(\theta)}{2} + d_A\right)\right). \text{ Eq. 3-25}$$

RRF is the fractional y-axis offset that occurs as one moves along the x-axis. This offset is due to the scan motion, combined with the pixel sub-elements being read sequentially (a so-called "rolling readout"). RRF is 0.016 in our case, meaning that for every unit distance moved in the x-direction, the element is shifted 0.016 units in the y-direction. In the above

expression, all the quantities other than the calibration offsets are either known or measured. Observations of several coastline crossings can therefore be used to solve for ΔX, ΔY, ϕ_A, and ϕ_B in a least-squares sense.

Once ΔX, ΔY, and ϕ_i are determined for each channel, the relative calibration is complete. These offsets define how all visible channels can be co-aligned. The accuracy of this calibration can be estimated from the equations derived above. If Eq. 3-25 is solved for one of the calibration parameters, and partial derivatives taken with respect to d_A, d_B, and the other three calibration parameters, an uncertainty estimate analogous to that of Eq. 3-23 can be found. The uncertainty in ΔX is given by

$$U_{\Delta X} = \frac{\tan\theta}{\tan\theta - RRF}\left[U_{dA}^2\left(1 + \frac{\phi_A}{RRF - \tan\theta}\right)^2 + U_{dB}^2\left(1 + \frac{\phi_B}{RRF - \tan\theta}\right)^2 + \frac{1}{\tan^2\theta}U_{\Delta Y}^2 + \right.$$

$$\left. + U_{\phi A}^2\left(\frac{\tan\theta + 2d_A}{2RRF - 2\tan\theta}\right)^2 + U_{\phi B}^2\left(\frac{\tan\theta + 2d_B}{2RRF - 2\tan\theta}\right)^2\right]^{1/2}. \quad \text{Eq. 3-26}$$

The U_i terms are the uncertainty associated with parameter i. If coastline crossings are made at an angle near 90 degrees, and if we assume the U_ϕ (in radians) are negligible compared to the U_d (in pixels), this simplifies to

$$U_{\Delta X} = U_{dA}\sqrt{\left(\frac{U_{dB}}{U_{dA}}\right)^2 + 1}, \qquad \text{Eq. 3-27}$$

which is $U_d\sqrt{2}$ if the two channels have the same noise level. The assumption that the U_ϕ terms are significantly less than the U_d is reasonable given that the ϕ angles are known to be less than 0.001 radians, while U_d are calculated to be ≥ 0.02 (Table 3.3).

The expression for $U_{\Delta Y}$ is similar, though it gets arbitrarily large for $\theta = 90°$, and is small for small θ. If an intermediate value of $\theta = 45°$ is assumed, if we choose a coastline for which d_A and d_B are small, and again taking $U_\phi < U_d$,

$$U_{\Delta Y} = \sqrt{2}U_{\Delta X} \qquad \text{Eq. 3-28}$$

The expressions for U_ϕ require simplification as well for error estimation. Taking $\theta = 90°$, and again assuming a relatively small value for U_ϕ, one arrives at the representative values

$$U_{\phi A} = U_{\phi B} = 2\sqrt{U_{dA}^2 + U_{dB}^2 + U_{\Delta X}^2}. \qquad \text{Eq. 3-29}$$

As before, the U_ϕ are in radians, U_{dA}, U_{dB}, and $U_{\Delta X}$ are in pixel lengths (dimensionless).

Tables 3.3 and 3.4 use the above equations along with appropriate parameter values to calculate the uncertainty in locating coastlines and in the spatial calibration parameters. For the calculation of radiances in Table 3.3, the atmosphere is assumed to contain no clouds, but does contain oceanic aerosols yielding a surface visibility at 0.55 micron of 23 km. The temperature and water vapor profiles correspond to a tropical atmosphere, and the solar zenith angle is 20 degrees. The land surface is assumed to be a mixture of equal parts sand and vegetation. The noise level for each channel was estimated by taking 1 percent of the radiance for a surface with albedo 0.4, which is the minimum performance requirement specified for these channels.

Channel	n (W/m²/ster)	R_L (W/m²/ster)	R_O (W/m²/ster)	U_d (pixels)
1	0.06	2.319	1.971	0.24
2	0.19	7.960	3.453	0.06
3	0.23	20.878	0.985	0.02
4	0.77	32.889	7.910	0.04

Table 3.3 - Coastline Location Uncertainty

Table 3.4 lists calibration uncertainties for a single coastline crossing. The uncertainty decreases as $\sqrt{N}$, where N is the number of crossings observed. This means, for example, that Channels 2, 3, and 4 can be co-aligned to an accuracy of 0.01 pixels with 64 observed crossings, and channel 4 can be aligned with the same accuracy using roughly 1200 crossings. The coastline crossings do not constrain ϕ well: it takes over 2 million coastline crossings to achieve the *a priori* uncertainty of 0.001 radians. Given this practical limit, our knowledge of a pixel's location in a 9-pixel array can never be better than 9*0.001 pixels, and observations of 1200 coastline crossings will optimize the relative calibration of all channels.

Parameter	Relative Uncertainty	
	Channels 2, 3, and 4[*]	Ch. 1 Relative to Ch. 4[†]
ΔX	0.06 pixels	0.24 pixels
ΔY	0.08 pixels	0.34 pixels
ϕ	0.16 radians[**]	0.50 radians[**]

[*] U_d is taken to be 0.04 pixels for each channel.
[†] U_d is taken to be 0.04 pixel for Ch. 4, 0.24 for Ch. 1.
[**] ϕ is actually known *a priori* to be less than 0.001 radians.

Table 3.4 – Spatial Calibration Uncertainty for a Single Coastline Crossing.

3.4.2 Absolute Spatial Calibration of the Visible Channels

The absolute spatial calibration of the visible channels can be determined by coastline crossings as described above. "Absolute Calibration" is used here to mean spatial offsets from the spacecraft boresight, which can bring us into a geocentric frame. To do this, instead of comparing two visible channels, a comparison is made between the predicted coastline and an actual channel's data.

The predicted coastline is based on spacecraft ephemeris and pointing information, and coastal maps. Using the spacecraft absolute pointing accuracy of 0.05° (which corresponds to 27% of a visible pixel) for U_{dA} in Eq. 3-27 and 3-28, and using U_{dB} from Table 3.3, the absolute spatial calibration for each channel can be calculated. Values are listed in Table 3.5. Note that the ϕ values from Table 3.4 are repeated here, since they are already referenced to an absolute frame.

Channel	ΔX (pixels)	ΔY (pixels)	ϕ^* (radians)
1	0.36	0.51	0.50
2	0.28	0.40	0.16
3	0.27	0.38	0.16
4	0.27	0.38	0.16

$^*\phi$ is actually known to 0.001 radians based on the instrument specifications.

Table 3.5 - Absolute Spatial Calibration Uncertainty for a Single Coastline Crossing

The absolute spatial calibration also improves by a factor of $\sqrt{N}$ as more crossings are used in the solution. To achieve an absolute calibration accuracy of 0.01 pixels for all channels will require observing approximately 2600 coastline crossings.

3.4.3 Spatial Calibration of Visible Channels to the Infrared

Excluding research products, the primary purpose of the visible channels is to provide statistical information on cloud structures and surface inhomogeneities within an infrared footprint. For these purposes, it is sufficient that the visible and IR instruments be aligned to within half of a visible pixel. The previous section has shown that, with a small number of coastal crossings (25), the visible channels can be located with respect to the spacecraft boresight to within 0.1 visible pixels (about 200 meters on the ground at nadir). If the IR footprint is located with respect to the boresight to within 0.49 visible pixels, then the combined visible to IR uncertainty will be less than 0.5 pixels.

An order-of-magnitude argument can be used to demonstrate that the coastline crossing technique described in Section 3.4.1, when applied to the footprint and signal characteristics of the infrared instrument, yields the required accuracy. Assuming Eq. 3-24 is approximately correct for the IR observations, taking the instrument noise to be 0.2 K (the maximum NEΔT in the instrument specifications), and using an ocean to land brightness temperature contrast of 10 K, the coastline location can be located to about 3% of the IR footprint size, or 17% of a visible pixel. Using Eq. 3-27, with U_{dA} being the boresight knowledge of 0.05° and U_{dB} being 17% of a visible pixel, it is found that the IR footprint can be located with respect to the spacecraft boresight to within 30% of a visible pixel. Thus, it appears that even a single coastline crossing achieves the desired accuracy. This conclusion is consistent with Section 2.4.1.

While this analysis is optimistic in assuming that the ocean and surface are homogenous on the 14 km scale of the infrared footprint, that the land/ocean radiance change occurs as a step function, and that the coastline is straight, any additional uncertainty these assumptions cause can be mitigated by using multiple coastline crossings.

3.4.4 Co-Alignment of the MODIS and AIRS Instruments

The MODIS instrument observes in the visible and infrared, with nadir spatial resolution of about 0.2 km at visible wavelengths, and 1 km in the infrared. (This corresponds to 0.09 to 0.45 of an AIRS visible pixel.) Pre-launch calibration of MODIS allows its orientation relative to the spacecraft boresight to be known to better than 0.2 MODIS pixels.

Some potential uses of MODIS data are improved radiometric calibration of the AIRS visible channels (Section 3.2.4), and statistical studies of variability on scales smaller than an AIRS visible pixel. For these purposes, alignment of AIRS and MODIS to 0.1 of an AIRS visible pixel (equivalent to one MODIS visible pixel) is sufficient. The values in Table 3.5 indicate that observations of 25 coastline crossings will determine AIRS visible offsets from the spacecraft boresight well enough to meet this 1/10-pixel accuracy using MODIS' pre-launch determination of its offsets from boresight. Similarly, a single coastline crossing observed by AIRS in the infrared should be sufficient to align MODIS and AIRS infrared data to within 1 MODIS infrared pixel.

3.4.5 Gridding and Mapping Considerations

While not formally a part of the Level 1b product, brief mention will be made of the following data processing tasks: mapping of visible data, combining of visible and infrared data, and visible data quality control.

3.4.5.1 Mapping of Visible Data

As the scan mirror rotates to view across track (Figure 3.1), the projection of each visible detector on the ground rotates and stretches due to geometric effects. A transform function will be derived that translates pixel element number and scan angle into geocentric coordinates. Because there is a one-pixel overlap between successive scans of the visible instrument at nadir, some surface points will be sampled twice. In such cases, each measurement will be tested to see if it is valid (see "Quality Control", below). If both samples are valid, their average value will be used. If one of the samples is invalid, it will be rejected, and the remaining measurement used. If both samples are invalid, they are both ignored, and the pixel in question is assigned the average value of its nearest neighbors for mapping purposes.

Once each channel of visible data is independently gridded, they will be aligned onto the grid of the reference channel, described in Section 3.4.1. This alignment will be a linear superposition, using the ΔX, ΔY, and ϕ offsets determined by coastline crossings.

3.4.5.2 Gridding of Visible and Infrared Data

The offsets between visible and infrared data, determined by the technique of Section 3.4.3, will be used to map the visible data onto the infrared's data grid. Unlike the pure visible case, however, the different footprints of the data sets must be accounted for. A beam pattern (or convolution function) will be calculated for the infrared data, and this smoothing applied to the visible data. The smoothed visible data can then be directly compared to the infrared.

3.4.5.3 Visible Data Quality Control

Charged particles striking the visible detectors can create spurious signals. Once the visible data is mapped, many "upset" pixels can be recognized by their large deviations from neighboring pixels. Whenever a visible map contains a pixel differing from the average value of its nearest neighbors by more than 3-sigma (sigma can be the noise estimate provided in Table 3.3 for each channel), that pixel will be rejected.

3.5 AIRS Visible/Near-Infrared Radiometric Calibration Software

What follows is a description of the steps which will be taken to perform the visible and near-infrared radiometric calibration of the AIRS instrument. We assume that the AIRS visible/near IR channels meet the specification described in the AIRS Functional Requirements Document (Ref. 2).

The first data regarding electronics linearity and detector noise will come from the flight unit testing in the summer of 1998. (The AIRS engineering unit does not include the visible

sensors.) With minor modifications, the algorithm used for the visible is the same as the one used in the infrared channels, described in Section 2.5.

3.5.1 Dataflow Description

Figure 3.14 shows a top-level diagram of the AIRS Visible/Near IR radiometric calibration dataflow, from level-1A engineering units (and ancillary data) through level-1B calibrated radiances. The steps can be summarized as follows:

a) Use internal blackbody views (the infrared calibration source) to determine detector offsets.

b) Use photometric calibration target views and calculated detector offsets to determine detector gains.

c) Apply pre-calculated multiplicative factors (based on measurements of ground truth) to produce corrected detector gains.

d) Use visible and near-IR scene data numbers and calculated detector offsets and gains to produce calibrated scene radiances.

3.5.2 Preliminary Processing Corrections

Some processing steps are performed on each and every data number (this includes scene views, blackbody views, and photometric calibration target views). Because these steps can be applied directly to the input data numbers (before beginning the offset and gain calculations) they are grouped together here as pre-processing corrections. At present the only correction which will be done this way is the linearity correction.

3.5.2.1 Linearity Correction

Prior to being used for processing, footprint data numbers (including scene views, space views, and gain views) are corrected for non-linearity. This consists of using a pre-calculated look-up table (probably generated from a polynomial) to adjust observed counts to a linearized output, henceforth referred to as "linearized counts". The data for this transformation come from pre-flight measurements, and may be updated based on in-orbit linearity assessments.
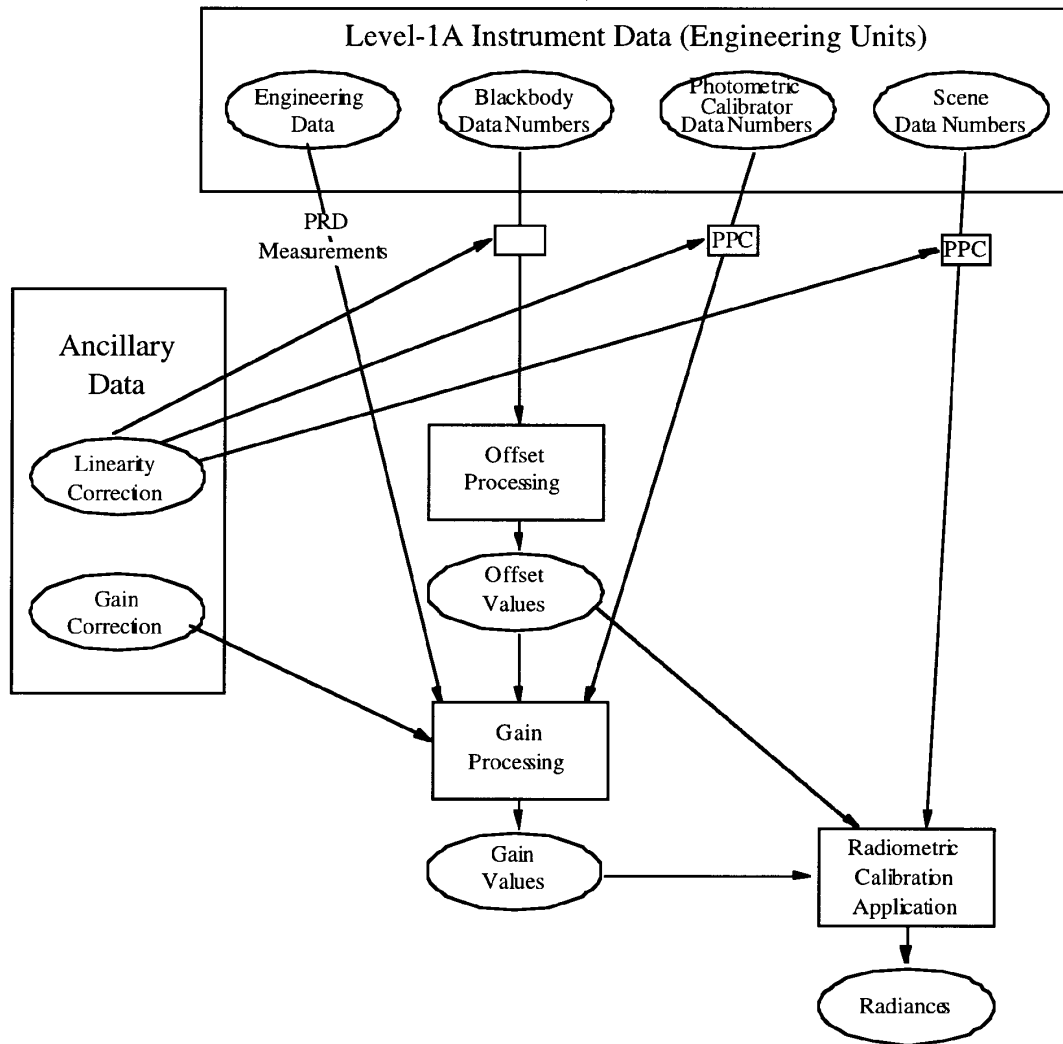
Figure 3.14

Data processing flow for VIS/NIR data

3.5.3 Offset Processing

Pre-processed blackbody views are used, for each VIS/Near-IR channel, to determine the instrument response to a zero-radiance scene (the 310 degree Kelvin blackbody produces no significant radiance in the VIS/Near-IR bands). This response is in units of counts (dn).

3.5.3.1 Offset Blackbody View Selection

There are currently no selection criteria for blackbody views for VIS/Near-IR offset processing. That is, it is currently expected that all views of the internal blackbody will be suitable for use as VIS/Near-IR offset calibration footprints.

3.5.3.2 Offset Fitting.

Because there is noise on the blackbody views, it is desirable to combine many dark views, thereby obtaining a $\sqrt{N}$ decrease in noise levels. (Beyond some time, on the order of 5 minutes (TBD), however, 1/f noise begins to dominate.) Because the offset level in each detector may change with time, it is desirable to fit to the smoothed variation in observed dark view counts, rather than simply taking an average.

3.5.3.3 Sliding Window Approach

Because we can assume that the true offset (and gain) of a detector at a given instant is reflected by measurements made close to that time, and because offset is subject to variation, it is clear that the best determination of instantaneous offset is made when the set of space views which are being fitted to are centered on the time of interest (assuming no data drop-outs).

By making this fitting "window" large (about five minutes), not only is the noise reduced, but a smoothing operation is also performed. Specifically, this approach can be expected to reduce the point-to-point variability of calculated offsets by as much as a factor of 10 (there being some 120 scan sets in five minutes).

3.5.4 Gain Processing

Pre-processed views of the internal photometric calibration target are combined with calculated offset values and photometric calibrator temperature measurements to determine each detector's gain.

3.5.4.1 Gain View Selection

Photometric calibration target views for which Precision Reference Diode (PRD) measurements exist are selected. In the absence of PRD measurements (i.e., if the engineering data packet is missing) no gain calculation can be done.

3.5.4.2 Photometric Target Radiance Calculation

The output of the photometric calibration target in absolute units (W/m^2), N_c, is determined directly from the outputs of the two PRDs using a table lookup.

3.5.4.3 Instantaneous Gain Calculation

If the detector electronics measures count V_c when viewing the internal photometric calibration target with radiance N_c, and measures count V_s when viewing the blackbody, the instantaneous detector gain is given by

$$G = \frac{N_c}{V_c - V_s}, \qquad\qquad\qquad \text{Eq. 3-30}$$

in W / m^2 /count.

3.5.4.4 Gain Fitting

Because there is noise on the gain calibration views, it is desirable to combine (N) gain views, thereby obtaining a $\sqrt{N}$ decrease in noise levels (up to a point). Because the gain of each detector is not expected to vary significantly during the two minutes when the photometric calibration lamp is on, it is acceptable to simply average the observed gain counts for a single two-minute calibration cycle. This produces (for each spectral channel) a single value of gain which is representative of the two-minute period.

For the two orbits between each photometric calibrator cycle, estimated gain will be fit to, relying on engineering measurements of the detector temperatures.

3.5.4.5 Gain Interpolation with Time

Because of the sparseness of the gain measurements (measured for just two minutes out of every two hundred minutes), the concept of windowing used for smoothing and time interpolating the dark views does not apply. The current plan is to simply interpolate between calibration cycles. In the event that the gains vary too much from orbit to orbit (thus introducing a discontinuity in the slope of the fit), a multi-orbit windowing approach can be taken.

3.5.4.6 Vicarious Gain Correction

Because of the large uncertainly associated with the calculated gain values (due to the 20% uncertainly in absolute radiance of the photometric targets), it is desirable to correct these gain values relying on ground truth (see Section 3.2.3). For purposes of the operational calibration algorithm, this correction consists simply of multiplying the calculated smoothed gain values by constant factors, $\gamma(g)$ and $\gamma(M)$, (different for each spectral channel). These correction factors are provided by the science team, and are a non-routine (research) product. The default value for the vicarious gain correction factors is 1.00 for all channels.

3.5.5 Radiometric Calibration Application

3.5.5.1 Two Point Calibration

Given the calculated offsets and gains, calibrated radiances (in units of W/m^2) are obtained directly by subtracting the calculated offsets from the pre-processed observed scene counts, and multiplying this difference by the calculated instrument gain (Section 3.2.4.3).

3.5.5.2 Polarization and Angle-dependent Scan Mirror Correction

No explicit scan angle-dependent corrections are necessary to the VIS/Near-IR radiances. (The polarization effect of the scan mirror, which can be important in the infrared, is negligible for the visible channels.)

3.6 Spectral Calibration Algorithm

There is no explicit on-board spectral calibration of the AIRS VIS/NIR instrument. Changes in the spectral system response are indirectly accounted for in $\gamma(g)$ and $\gamma(M)$.

3.7 Quality Control/Error Estimates/Exception Handling

3.7.1 Quality Control

Quality of level-1B products is ensured primarily by the routine analysis of the level-2 products of selected ground sites which are observed as part of the normal spatial coverage. The algorithm for this task is a team member research product.

3.7.2 Error Estimates

Uncertainties in the level-1B products (offsets, gains, and radiances) are quantified based on two primary indicators and one secondary indicator. The first primary indicator is the quality of the fits that are done to offset and gain. These quality indicators are in the form of "correlation coefficients". The second primary quality indicator is the availability of calibration data. If many blackbody footprints are missing over the desired five minute interval, we know that the noise level will be higher. This concept will be developed quantitatively using experience gained with the flight model.

A secondary indicator of data uncertainty is the magnitude of the discrepancy between the routinely produced data from a ground calibration site and the truth. The algorithm for this estimate is a research task of an AIRS team member.

3.7.3 Exception Handling

Because the level-1A processing will have analyzed the quality of the instrument telemetry (testing for completeness and corruption), no garbled data should be processed. The only exception currently anticipated is the possibility of data drop-outs (gaps), and the impact of these on level-1B processing is minimal. If scene footprints are missing, they are simply not calibrated. If offset (blackbody) calibration footprints are missing, there should be plenty of others within the five minute window with which to work. If gain (photometric calibrator) calibration footprints are missing, the most recent good data will be used instead, and the quality indicators will be modified accordingly. The only exception for which actual handling is done is the ability to begin and end processing smoothly when gaps longer than five

minutes are encountered. Other exceptions (notably spurious data) can be handled in the footprint selection or mapping routines (see Sections 3.4.5.3, 3.5.3.1, 3.5.4.1, and 3.5.5.1) as required.

3.8 References for Section 3

Abel P., (1991), Clouds As Calibration Targets For AVHRR Reflected-solar Channels: Results From a Two-year Study At NOAA/NESDIS, SPIE, Vol. 1493, 195-206

Brest C. L. and W. B. Rossow, (1992), Radiometric Calibration and Monitoring of NOAA AVHRR Data For ISCCP, Int. J. Remote Sensing, Vol. 13, No. 2, 235-273

Che N., B. G. Grant, D. E. Flittner, P. N. Slater and S. F. Bigger, (1991), Results of Calibration of the NOAA-11 AVHRR Made By Reference To Calibrated SPOT Imagery At White Sands, N. M., SPIE, Vol. 1493, 182-194

Che N and J. C. Price, (1992), Survey of Radiometric Calibration Results and Methods For Visible and Near-Infrared Channels of NOAA-7, -9 and -11 AVHRRs, Remote Sensing of Environment, 41, 19-27

Fraser R. S. and Y. J. Kaufman, (1985), Calibration of Satellite Sensors After Launch, Applied Optics, Vol. 25, No. 7, April, 1986

Frouin, R., and Gautier C., (1987), Calibration of NOAA-7, GOES-5 and GOES-6 VISSR/VAS Solar Channels, Remote Sensing of Environment, 22, 73-101

Guenther, B. W., Gilmore, R., Markham, B.L., and Cooper, J., (1990), Result From the NASA ER-2 Aircraft Experiment at White Sand, N.M., Meeting on Radiometric Calibration of Satellite Sensors of Reflected Solar Radiation. NOAA/NESDIS, March 27-28

Holben B. N., Y. J. Kaufman and J. D. Kendall, (1990), NOAA-11 AVHRR Visible and Near-IR Inflight Calibration, Int. J. Remote Sensing, Vol.11, No. 8, 1511-1519

Jones, M., H. Montgomery, R. Veiga, D. Knowles, N. Che and I. L. Goldberg, MODIS Level 1B Algorithm Theoretical Basis Document 1995 [MOD-02].GSFC, SBRC

Price J. C., (1987), Radiometric Calibration of Satellite Sensors in the Visible and Near-Infrared: History and Outlook Int. J. Remote Sensing, 22, 3-9

Ricchiazzi P., S. Yang and C. Gautier, (1996), SBDART: A Practical Tool for Plane-Parallel Radiative Transfer in the Earth's Atmosphere, Computers & Geosciences (submitted 5/96)

Slater, P.N., S. F. Biggar, J. M. Palmer, (1991), Ground-reference Site and On-board Method For Sensor Absolute Calibration in the 0.4 to 2.5 μm Range, Proc. Helsinki IGARRS'91, June

Slater, P.N., S. F. Biggar, R. G. Holm, R. D. Jackson, Y. Mao, M. S. Moran, J. M. Palmer, and B. Yuan, (1987), Reflectance- and Radiance-based Methods for the In-flight Absolute Calibration of Multispectral Sensors, Remote Sensing of Environment, 22, 11-37

Walraven R. L. and Coulson K. L. (1972), Measurements of Light Properties of Gypsum Sand, contrib. Atmos. sci., No. 7, Univ. of California, Davis.